Inorganic Chemistry

ARTICLE

pubs.acs.org/IC

Temperature Dependence of the Crystal Structure and *g*-Values of *trans*-Diaquabis(methoxyacetato)Copper(II): Evidence for a Thermal Equilibrium Between Complexes with Tetragonally Elongated and Compressed Geometries

Charles J. Simmons,[*,†] Horst Stratemeier,[‡] Michael A. Hitchman,[*,‡] Dirk Reinen,[§] Vanessa M. Masters,[∥] and Mark J. Riley[*,∥]

[†]Division of Natural Sciences, University of Hawaii at Hilo, Hilo, Hawaii 96720-4091, United States

[‡]School of Chemistry, University of Tasmania, Box 252-75 Hobart, Tasmania 7001, Australia

[§]Fachbereich Chemie der Universität Marburg, Universität Marburg, Hans-Meerwein Strasse, D-3550 Marburg, Germany

[∥]School of Chemistry and Molecular Biosciences, University of Queensland, St. Lucia, Queensland 4072, Australia

Supporting Information

ABSTRACT: The crystal structures of *trans*-diaquabis-(methoxyacetato)copper(II) and the isostructural nickel(II) complex have been determined over a wide temperature range. In conjunction with the reported behavior of the *g*-values, the structural data suggest that the copper(II) compound exhibits a thermal equilibrium between three structural forms, two having orthorhombically distorted, tetragonally elongated geometries but with the long and intermediate bonds to different atoms, and the third with a tetragonally compressed geometry. This is apparently the first reported example of a copper(II) complex undergoing an equilibrium between tetragonally elongated and compressed forms. The optical spectrum of single crystals of the copper(II) compound is used to obtain metal−ligand bonding parameters which yield the *g*-values of the compressed form of the complex and hence the proportions of the complex in each structural form at every temperature. When combined with estimates of the Jahn−Teller distortions of the different forms, the latter produce excellent agreement with the observed temperature dependence of the bond lengths. The behavior of an infrared combination band is consistent with such a thermal equilibrium, as is the temperature dependence of the thermal ellipsoid parameters and the XAFS. The potential surfaces of the different forms of the copper(II) complex have been calculated by a model based upon Jahn−Teller coupling. It is suggested that cooperative effects may cause the development of the population of tetragonally compressed complexes, and the crystal packing is consistent with this hypothesis, though the present model may oversimplify the diversity of structural forms present at high temperature.

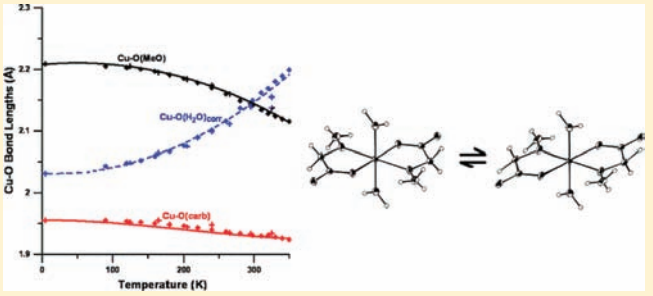

INTRODUCTION

The stereochemistry of copper(II) complexes is generally interpreted in terms of Jahn−Teller (JT) vibronic coupling,[1] this being termed "dynamic" when the geometry and electronic structure change with temperature.[2] Interest in this area has been stimulated by the proposal that the behavior of high-temperature superconductors may depend upon such effects.[3] Moreover, certain copper "blue" proteins exhibit temperature dependent properties which may also be caused by dynamic vibronic coupling.[4] Dynamic behavior may occur when a complex is localized in one state, with a higher state admixed into this by a mechanism analogous to that providing the intensity in Laporte−forbidden electronic transitions,[5] though such behavior is rare. Dynamic behavior is usually associated with an E⊗e Jahn−Teller ground state potential surface warped by higher-order effects and interactions with the surrounding crystal lattice to give three minima having different energies. At very low temperatures, the complex is generally completely localized in the lowest-energy minimum with dynamic behavior at higher temperatures resulting from thermal population of the second vibronic minimum, the third minimum being too high in energy to be involved. The geometry difference between the two levels usually involves interchange of the directions of the long and intermediate bonds in the complex, so that thermal population of the upper state causes the average length of these bonds and the *g*-values along these directions to vary with temperature. Experimentally, the changes in geometry are revealed by X-ray or neutron diffraction,[6]

Received: January 19, 2011
Published: May 03, 2011

and the change in wave function is deduced from the temperature dependence of the electron paramagnetic resonance (EPR) spectrum.[2,5] The underlying cause of such thermal behavior was first recognized by Silver and Getz,[7] who developed a simple approach (the SG model) based upon Boltzmann statistics to interpret the temperature dependence of the *g*-values observed for Cu^{2+} doped $K_2[Zn(H_2O)_6](SO_4)_2$.

A more detailed treatment to interpret the properties of "fluxional" copper(II) complexes has been developed by Riley et al.[8] (the RHW model). This model was used initially to interpret the temperature-dependent *g*-values of six-coordinate complexes in terms of second-order JT coupling and ligand inequivalence[9] and the change in bond lengths and thermal ellipsoid parameters observed in X-ray and neutron diffraction studies of dynamic pure copper(II) compounds.[10] A similar approach was used to interpret the behavior of a chromium(II) complex.[11] Sometimes, both structural forms are present even after cooling to 4 K, which has led to incorrect conclusions concerning the geometry and ground state wave function of the complex.[12] Measurement of the X-ray absorption fine structure (XAFS) has proved valuable for such systems, as this reveals the *local* bond lengths of a complex.[13] In the case of $(ND_4)_2[Cu(D_2O)_6](SO_4)_2$, the basic assumption that the thermal behavior is due to an equilibrium between complexes differing only by the interchange of bond directions was confirmed by showing that the XAFS does not alter significantly between 5 and 298 K.[14] However, the detailed thermal behavior of $(ND_4)_2[Cu(D_2O)_6](SO_4)_2$ cannot be explained satisfactorily by either the SG or the RHW model. It was suggested that this is because the difference in geometry of the thermally excited complexes alters the lattice strain experienced by their neighbors, and a model based upon such cooperative interactions successfully explained the observed behavior.[15]

The compound *trans*-diaquabis(methoxyacetato)copper(II), $[Cu(MeOAc)_2(H_2O)_2]$, has been the subject of several previous studies, the most recent involving a molecular modeling study of the infrared spectrum.[16] Its crystal structure was first determined at room temperature by Prout et al.[17] and at 125 K by Hathaway.[18] Prout et al. subsequently redetermined its structure at eight different temperatures between 4.2 and 325 K.[19] The asymmetric unit consists of one centrosymmetric molecule and at low temperature this has a tetragonally elongated octahedral geometry with a modest orthorhombic distortion. As the temperature is raised, the bond of intermediate length, Cu−O4(water), apparently increases while the longest bond, Cu−O3(methoxy), decreases, until by room temperature they actually cross, so that at high temperature the complex appears to adopt a tetragonally compressed octahedral geometry. Initially, the optical and EPR spectra were interpreted using this geometry, inferring that at room temperature the unpaired electron resides largely in the d_{z^2} orbital.[20] However, subsequent investigations concluded that the ground state lies midway between those expected for geometries of tetragonally compressed and elongated octahedra.[21] A later study of the temperature dependence of the EPR spectrum[22] deduced that at low temperature the ground state wave function is dominated by the $d_{x^2-y^2}$ orbital, consistent with the orthorhombically distorted, tetragonally elongated octahedral geometry indicated by its crystal structure. However, the *g*-values change dramatically upon raising the temperature to 344 K, the two higher *g*-values almost converging, and it was concluded that this is probably caused by a SG-type dynamic equilibrium.[22] A similar conclusion was drawn from the analysis of the temperature dependence of the crystal structure.[19] Particularly important is the significant increase of the thermal difference displacements of the O3(MeO) and O4(H_2O) atoms in the directions of the bonds to the copper(II) ion, ΔU_{obs}(Cu−O). Such an increase is not observed for the isostructural nickel(II) compound, implying that a thermally generated disorder of the water and methoxy groups occurs for the copper(II) complex as required by the SG model.

While the above evidence clearly implies that $[Cu(MeOAc)_2(H_2O)_2]$ exhibits a dynamic thermal equilibrium involving the bonds to the water and methoxy groups, careful inspection of the reported data suggests that an interpretation solely in terms of a SG-type mechanism is inadequate. Such a mechanism requires that the lowest *g*-value and shortest Cu-(ligand) bond length should not vary significantly with temperature, and this is so for the many compounds which exhibit such behavior.[2,6] However, the lowest *g*-value of $[Cu(MeOAc)_2(H_2O)_2]$ decreases from 2.04_5 at 4.2 K to 2.02_3 at 344 K; hyperfine splitting was not resolved.[22] While this change may seem modest, it represents a substantial decrease in the g-shift from the free-electron value of 2.00, implying a significant drop in the orbital angular momentum of the unpaired electron.[23] This suggests that at high temperature the unpaired electron spends a significant time in the copper(II) d_{z^2} orbital, since, to first order, such an occupancy causes no axial g-shift.[23] A d_{z^2} ground state orbital is associated with a tetragonally compressed octahedral coordination geometry, and indeed for $[Cu(MeOAc)_2(H_2O)_2]$, the Cu−O1(carboxylate) bonds, which would lie along the short axis of such a polyhedron, do decrease somewhat as the temperature rises. An axially compressed geometry is rather rare for Cu(II) complexes and the factors influencing its adoption are discussed in refs 1 and 5.

The simplest explanation of the thermal behavior of $[Cu(MeOAc)_2(H_2O)_2]$ would be a gradual change toward a compressed geometry for all the complexes. However, a uniform change of this kind is incompatible with the observed increase in thermal difference displacement parameters, which implies a thermal equilibrium involving two or more structures having bonds of different length to the water and methoxy groups. Moreover, it will be shown that the XAFS does not converge for the Cu(II) complex at high temperatures, which is consistent with the presence of complexes having quite different metal−ligand bond lengths in this temperature region, rather than simply an interchange of medium and long bonds.

A possible explanation for the EPR and diffraction results is that $[Cu(MeOAc)_2(H_2O)_2]$ exists in a single molecular form with an orthorhombically distorted tetragonally elongated octahedral geometry at 4.2 K, but that at ~350 K, a dynamic equilibrium occurs involving a form having a tetragonally compressed octahedral geometry. This would represent a new kind of structural behavior, as previous thermal equilibria observed for Cu(II) compounds all involve different levels of a single potential surface, that of the orthorhombically distorted, tetragonally elongated octahedron commonly observed for this metal ion. To investigate this hypothesis, the structural data have been extended by accurately redetermining the crystal structure of $[Cu(MeOAc)_2(H_2O)_2]$ by X-ray diffraction over as wide a temperature range as possible. The crystal structure of the corresponding isostructural nickel(II) compound[24] has also been studied over a wide temperature range to observe the behavior of the analogous complex of a non-Jahn−Teller-active metal ion. The visible and near-infrared spectrum of a single crystal of the

copper(II) compound has been measured over a temperature range to deduce bonding parameters for the ligand atoms and to look for evidence of a thermal equilibrium. XAFS spectra have been recorded over a temperature range for the two compounds. The *g*-values expected for $[Cu(MeOAc)_2(H_2O)_2]$ in the tetragonally compressed form were estimated and used to deduce the proportion of complexes in this form at each temperature. The *g*-values of the complexes remaining in the tetragonally elongated form were also estimated at each temperature, and their behavior analyzed in terms of a SG-type equilibrium. The possibility that cooperative interactions may influence the equilibria has been evaluated by studying the crystal packing of the complexes. The temperature dependence of the Cu−O bond lengths and difference displacement parameters have been estimated and the potential surfaces of the different forms calculated using the RHW model.

EXPERIMENTAL SECTION

Preparation of Compounds. Crystals of $[Cu(MeOAc)_2(H_2O)_2]$ and $[Ni(MeOAc)_2(H_2O)_2]$ were prepared as described previously and had satisfactory analyses.[17]

X-ray Crystal Structure Determinations. Suitable crystals of the copper and nickel compounds were ground to spheres of approximate radius 0.30 mm and mounted on the tips of glass fibers with quick-drying epoxy glue. All X-ray diffraction data were collected using graphite monochromated Mo Kα radiation (λ = 0.71069 Å) on a Nonius Kappa CCD diffractometer equipped with an Oxford Model 700 Cryostream cooler. Sixteen data sets from 90 to 350 K were obtained for the copper compound and six data sets from 100 to 350 K were obtained for the nickel compound. Each data set was measured using a combination of φ and ω scans with κ offsets. The data frames were integrated and scaled using the HKL suite of XdisplayF, Denzo and Scalepack.[25a] Unit cell parameters were retrieved and refined on all observed reflections. The structures were solved by direct methods and refined by full-matrix least-squares on F using teXsan for Windows v. 1.06.[25b] All nonhydrogen atoms were refined with anisotropic thermal parameters. Hydrogen atoms were located in Fourier difference maps and refined with isotropic thermal parameters. Crystallographic data and structural refinements for all 22 data sets are summarized in Tables 1 and 2; important metal−oxygen bond lengths and differences in mean-square displacements between the metal and O ligand atoms along the metal−oxygen bonds, ΔU_{obs}(M-O), calculated from the anisotropic displacement parameters using PLATON for Windows,[25c] are listed in Tables 3 and 4. An ORTEP drawing of $[Cu(MeOAc)_2(H_2O)_2]$ is shown in Figure 1. Bond lengths and angles for all 22 data sets are available in CIF format.

Electronic Spectra. Single crystal optical spectra of the copper compound were recorded between 12 and 298 K on a Cary 5A spectrophotometer by a method described previously,[26] the sample being cooled using a Cryodyne model 21 cryostat. No significant polarization of the bands was observed, so unpolarized light was used, and the crystal morphology was not determined. The temperature dependence of the optical spectrum of the compound was also measured to evaluate ligand bonding parameters and to look for effects due to the proposed structural equilibrium. The spectra are shown in Figure 2.

XAFS. X-ray absorption measurements for both compounds were made in transmission mode at the Australian National Beamline Facility (ANBF) on bending-magnet beamline 20B at the KEK Photon Factory, Tsukuba, Japan. The XAFS were recorded at six temperatures between 12 and 298 K using an Oxford Instruments closed cycle cryostat, with other experimental conditions given in Supporting Information (S-1) and spectra in (S-2).

RESULTS AND DISCUSSION

Procedure Used to Investigate the Thermal Equilibrium. The problem of concern is the interpretation of the temperature dependence of the structure and EPR spectrum of $[Cu(MeOAc)_2(H_2O)_2]$; see Figure 3. At low temperature the complex is uniformly in the tetragonally elongated form, with a slight orthorhombic distortion, and the optical spectrum has been used to calculate metal−ligand bonding parameters with this geometry. The likely structure of the compressed tetragonal form of $[Cu(MeOAc)_2(H_2O)_2]$ is estimated, and the changes in bond length compared with the elongated form have been used to derive the bonding parameters, and hence the proportion of the complex with this geometry at each temperature, as well as the *g*-values of the complexes remaining in the elongated form. The latter are found to vary significantly with temperature in a manner suggesting that the tetragonally elongated complexes undergo a SG-type thermal equilibrium, and the proportion of each structural type has been determined as a function of temperature. The Cu−O bond lengths and the difference displacement parameters of each ligand atom along the Cu−O bond were estimated from the proportion of the forms at each temperature and compared with experiment. The XAFS of the copper(II) and nickel(II) compounds were measured at various temperatures to look for evidence of the proposed equilibria. The temperature dependence of the *g*-values of the complexes with a tetragonally elongated geometry has been analyzed within the framework of a SG-type equilibrium, and the cause of deviations from the simple form of this model is discussed. The RHW model has been used to deduce the potential surfaces of the complexes involved in the thermal equilibria. The form of each potential surface depends upon the strain experienced by the complex, and this is discussed in terms of the nature of the ligands and interactions with neighboring complexes, providing an insight into the underlying cause of the unusual thermal equilibrium.

X-ray Crystal Structures. The crystals are built up from units of $[M(MeOAc)_2(H_2O)_2]$ with the M(II) ions located at inversion centers. The coordinated water molecules are hydrogen-bonded to carbonyl oxygen atoms O2 and O2* on neighboring complexes and vice versa so that are there are eight hydrogen-bonding contacts per complex to six-nearest neighbors, the only intermolecular interactions other than van der Waals contacts in the crystal (see Figure 4). In particular, the H4A* water atom is about 0.6 Å out of the $O2^{ii}$, $C1^{ii}$, and $O1^{ii}$ plane, and the hydrogen bond, 2.79−2.80 Å long, is approximately parallel to the $C1^{ii}$-$C2^{ii}$ bond vector and nearly perpendicular to the $C1^{ii}$-$O1^{ii}$ bond vector, whereas the H4B* atom is about 0.8 Å out of the $O2^{i}$, $C1^{i}$, and $O1^{i}$ plane (on the opposite side with respect to H4A*), and the hydrogen bond, 2.77−2.81 Å, is roughly parallel to the $C1^{i}$-$O1^{i}$ bond vector. The fact that the only significant interactions between a given complex and its neighbors is through the coordinated water molecules and carbonyl oxygen atoms of neighboring molecules, suggests that the significant increase in Cu−O(H_2O) bond lengths, which occurs when a complex is thermally excited to the upper state in the SG-type equilibrium, is accompanied by an increase in strain acting on the Cu−O(carb) bonds of these neighbors.

Estimation of the Geometry of the Complexes involved in the Thermal Equilibrium. We need to take into account bond length differences due to different types of ligand atom and lattice strain interactions. It is assumed that these will be reflected in the bond lengths observed in the analogous isostructural Ni(II) complex where Jahn−Teller (JT) effects are absent. Here,

Table 1. Crystal and Refinement Data for *trans*-Diaquabis(methoxyacetato)copper(II)

	T = 90 K	T = 120 K	T = 140 K	T = 160 K	T = 180 K
formula	$C_6H_{14}CuO_8$	$C_6H_{14}CuO_8$	$C_6H_{14}CuO_8$	$C_6H_{14}CuO_8$	$C_6H_{14}CuO_8$
Fw	277.72	277.72	277.72	277.72	277.72
wavelength (Å)	0.71069	0.71069	0.71069	0.71069	0.70169
crystal system	monoclinic	monoclinic	monoclinic	monoclinic	monoclinic
space group	$P2_1/n$	$P2_1/n$	$P2_1/n$	$P2_1/n$	$P2_1/n$
a (Å)	6.8975(1)	6.9021(1)	6.9053(1)	6.9084(1)	6.9132(1)
b (Å)	9.8576(2)	9.8811(2)	9.8990(2)	9.9204(2)	9.9450(2)
c (Å)	7.1974(1)	7.1983(1)	7.1995(1)	7.2012(1)	7.2035(1)
β (deg)	95.7136(11)	95.7264(12)	95.7451(12)	95.7836(12)	95.8447(12)
V (Å^3)	486.94(1)	488.48(1)	489.65(1)	491.02(1)	492.68(1)
Z	2	2	2	2	2
d_{calc} (g cm^{-3})	1.894	1.888	1.883	1.878	1.872
crystal size (mm)	sphere 0.30	sphere 0.30	sphere 0.30	sphere 0.30	sphere 0.30
$F(000)$	286	286	286	286	286
abs. coeff (mm^{-1})	2.27	2.26	2.25	2.25	2.24
2θ range (deg)	4.14−71.20	4.12−71.24	4.12−71.22	4.12−71.20	4.10−71.20
index ranges (h, k, l)	−11/11,−15/16,−11/11	−11/11,−16/16,−11/11	−11/11,−16/16,−11/11	−11/11,−16/16,−11/11	−11/11,−15/16,−11/11
no. refl. collected	4439	4449	4444	4475	4490
no. unique refl.	2353	2354	2357	2367	2370
R equivalent refl.	0.012	0.011	0.011	0.011	0.013
data completeness	0.998	0.996	0.996	0.998	0.997
GOF[a] on F	1.99	1.99	1.97	1.97	1.99
No. refl. > 4$\sigma(I)$	1838	1825	1796	1771	1751
R_1 [I > 4$\sigma(I)$][b]	0.0183	0.0183	0.0185	0.0193	0.0198
wR_2 [I > 4$\sigma(I)$][c]	0.0220	0.0220	0.0220	0.0220	0.0220
extinct. coefficient	5.45×10^{-6}	4.92×10^{-6}	5.69×10^{-6}	5.51×10^{-6}	6.39×10^{-6}
largest diff. peak and hole (e Å^{-3})	0.56/−0.33	0.51/−0.39	0.48/−0.29	0.46/−0.37	0.43/−0.33
	T = 200 K	T = 220 K	T = 240 K	T = 260 K	T = 280 K
formula	$C_6H_{14}CuO_8$	$C_6H_{14}CuO_8$	$C_6H_{14}CuO_8$	$C_6H_{14}CuO_8$	$C_6H_{14}CuO_8$
Fw	277.72	277.72	277.72	277.72	277.72
wavelength (Å)	0.71069	0.71069	0.71069	0.71069	0.70169
crystal system	monoclinic	monoclinic	monoclinic	monoclinic	monoclinic
space group	$P2_1/n$	$P2_1/n$	$P2_1/n$	$P2_1/n$	$P2_1/n$
a (Å)	6.9192(1)	6.9257(10	6.9339(1)	6.9422(1)	6.9527(1)
b (Å)	9.9734(2)	10.0051(2)	10.0378(2)	10.0719(2)	10.1099(2)
c (Å)	7.2068(1)	7.2106(1)	7.2156(1)	7.2206(1)	7.2265(1)
β (deg)	95.9395(12)	96.0558(12)	96.1884(11)	96.3382(12)	96.5186(12)
V (Å^3)	494.66(1)	496.85(1)	499.29(1)	501.79(2)	504.67(2)
Z	2	2	2	2	2
d_{calc} (g cm^{-3})	1.864	1.856	1.847	1.838	1.827
crystal size (mm)	sphere 0.30	sphere 0.30	sphere 0.30	sphere 0.30	sphere 0.30
$F(000)$	286	286	286	286	286
abs. coeff (mm^{-1})	2.23	2.21	2.21	2.20	2.19
2θ range (deg)	4.08−71.24	4.08−71.22	4.06−71.22	4.04−80.48	4.04−71.22
index ranges (h, k, l)	−11/11,−16/16,−11/11	−11/11,−16/16,−11/11	−11/11,−16/16,−11/11	−11/11,−16/16,−11/11	−11/11,−15/16,−11/11
no. refl. collected	4521	4548	4565	4589	4553
no. unique refl.	2391	2393	2411	2421	2428
R equivalent refl.	0.012	0.013	0.011	0.013	0.015
data completeness	0.999	0.997	0.999	0.730	0.996
GOF[a] on F	1.95	1.99	1.99	1.97	1.95
no. refl. > 4$\sigma(I)$	1727	1693	1687	1584	1559
R_1 [I > 4$\sigma(I)$][b]	0.0202	0.0208	0.0205	0.0221	0.0219

dx.doi.org/10.1021/ic200554f |*Inorg. Chem.* 2011, 50, 4900–4916

Table 1. Continued

	T = 200 K	T = 220 K	T = 240 K	T = 260 K	T = 280 K
wR_2 [$I > 4\sigma(I)$][c]	0.0220	0.0230	0.0210	0.0220	0.0230
extinct. coefficient	6.282×10^{-6}	6.77×10^{-6}	8.08×10^{-6}	6.65×10^{-6}	7.22×10^{-6}
largest diff. peak and hole (e Å^{-3})	0.42/−0.31	0.38/−0.35	0.35/−0.30	0.38/−0.35	0.39/−0.24

	T = 298 K	T = 310 K	T = 320 K	T = 330 K	T = 340 K	T = 350 K
formula	$C_6H_{14}CuO_8$	$C_6H_{14}CuO_8$	$C_6H_{14}CuO_8$	$C_6H_{14}CuO_8$	$C_6H_{14}CuO_8$	$C_6H_{14}CuO_8$
Fw	277.72	277.72	277.72	277.72	277.72	277.72
wavelength (Å)	0.71069	0.71069	0.71069	0.71069	0.70169	0.70169
crystal system	monoclinic	monoclinic	monoclinic	monoclinic	monoclinic	Monoclinic
space group	$P2_1/n$	$P2_1/n$	$P2_1/n$	$P2_1/n$	$P2_1/n$	$P2_1/n$
a (Å)	6.9599(2)	6.9683(2)	6.9743(2)	6.9802(2)	6.9861(2)	6.9915(2)
b (Å)	10.1405(3)	10.1628(2)	10.1814(2)	10.2012(3)	10.2180(2)	10.2329(4)
c (Å)	7.2321(1)	7.2379(1)	7.2424(1)	7.2470(2)	7.2517(2)	7.2565(2)
β (deg)	96.6738(14)	96.7817(13)	96.8795(14)	96.9767(16)	97.0687(15)	97.1665(20)
V (Å^3)	506.96(2)	508.98(2)	510.57(2)	512.21(2)	513.72(2)	515.10(3)
Z	2	2	2	2	2	2
d_{calc} (g cm^{-3})	1.819	1.812	1.806	1.801	1.795	1.790
crystal size (mm)	sphere 0.30	sphere 0.30	sphere 0.30	sphere 0.30	sphere 0.30	sphere 0.30
F(000)	286	286	286	286	286	286
abs. coeff (mm^{-1})	2.18	2.17	2.16	2.15	2.15	2.14
2θ range (deg)	4.02−71.20	4.02−71.30	4.00−71.20	4.00−71.30	4.00−71.20	3.98−71.24
index ranges (h, k, l)	−11/11,−16/16, −11/11	−11/11,−16/16, −11/11	−11/11,−16/16, −11/11	−11/11,−15/16, −11/11	−11/11,−15/16, −11/11	−11/11,−14/16, −11/11
no. refl. collected	4622	4579	4629	4541	4559	4337
no. unique refl.	2445	2457	2453	2463	2472	2436
R equivalent refl.	0.012	0.016	0.015	0.022	0.019	0.031
data completeness	0.998	0.996	0.997	0.991	0.995	0.975
GOF[a] on F	1.97	1.99	1.95	1.98	1.99	1.90
no. refl. > $4\sigma(I)$	1514	1473	1370	1228	1175	968
R_1 [$I > 4\sigma(I)$][b]	0.0217	0.0230	0.0229	0.0237	0.0235	0.0242
wR_2 [$I > 4\sigma(I)$][c]	0.0220	0.0230	0.0220	0.0250	0.0230	0.0260
extinct. coefficient	6.22×10^{-6}	6.73×10^{-6}	6.90×10^{-6}	6.15×10^{-6}	4.81×10^{-6}	2.45×10^{-6}
largest diff. peak and hole (e Å^{-3})	0.39/−0.22	0.33/−0.28	0.27/−0.30	0.27/−0.26	0.27/−0.23	0.29/−0.21

[a] GOF = goodness-of-fit = $[\Sigma(|F_o| - |F_c|)^2/(m-p)]^{1/2}$ where m is the number of reflections and p the number of variables. [b] $R_1 = \Sigma||F_o| - |F_c||/\Sigma|F_o|$. [c] $wR_2 = [\Sigma w(|F_o| - |F_c|)^2/\Sigma w|F_o|^2]^{1/2}$, $w = 1/\sigma^2(F_o)$.

differences from the average metal−ligand bond length, δ, estimated using the structure at 100 K (see Table 4) are Ni−O(carb) = −0.0203 Å; Ni−O(MeO) = −0.0028 Å; and Ni−O(H_2O) = 0.0232 Å. Applying these values to the average bond length of the Cu(II) complex, one obtains the hypothetical structure of [$Cu(MeOAc)_2(H_2O)_2$] in the absence of a Jahn−Teller effect. When compared with the actual experimental (4 K) Jahn−Teller structure,[19] the differences δ' are obtained:

	no JT	including JT	δ'
Cu-O(carb)	2.045 Å	1.955 Å	−0.090 Å
Cu-O(MeO)	2.062 Å	2.209 Å	0.147 Å
Cu-O(H_2O)	2.088 Å	2.031 Å	−0.057 Å

(1)

To a first approximation for a tetragonally elongated complex, the JT model suggests that the ligands along z move out by 2 units and those along x and y move in by 1 unit compared with the geometry in the absence of vibronic coupling; the sign of the distortion is simply reversed for a tetragonal compression.[1] Neglecting the orthorhombic distortion, the above values of δ' imply that 1 unit of distortion for the complex is about 0.073 Å. Thus, to go from a complex elongated along the Cu−O(MeO) bond to one compressed along the Cu−O(carb) bond, both these bonds contract by 1 unit, while the Cu−O(H_2O) bond elongates by 2 units. This leads to the following estimated bond lengths for the tetragonally compressed form of [$Cu(MeOAc)_2(H_2O)_2$]:

$$\text{Cu-O(carb)} \quad 1.955 - 0.073 = 1.882 \text{ Å} \qquad (2)$$

$$\text{Cu-O(MeO)} \quad 2.209 - 0.073 = 2.136 \text{ Å}$$

$$\text{Cu-O}(H_2O) \quad 2.031 + 0.146 = 2.177 \text{ Å}$$

In a SG-type equilibrium, the upper state has the distortions reversed for the long and intermediate bonds. In this case this means that for the upper state of the tetragonally elongated

dx.doi.org/10.1021/ic200554f |Inorg. Chem. 2011, 50, 4900–4916

Table 2. Crystal and Refinement Data for *trans*-Diaquabis(methoxyacetato)nickel(II)

	T = 100 K	T = 150 K	T = 200 K	T = 250 K	T = 300 K	T = 350 K
formula	$C_6H_{14}NiO_8$	$C_6H_{14}NiO_8$	$C_6H_{14}NiO_8$	$C_6H_{14}NiO_8$	$C_6H_{14}NiO_8$	$C_6H_{14}NiO_8$
Fw	272.87	272.87	272.87	272.87	272.87	272.87
wavelength (Å)	0.71069	0.71069	0.71069	0.71069	0.70169	0.70169
crystal system	monoclinic	monoclinic	monoclinic	monoclinic	monoclinic	monoclinic
space group	$P2_1/n$	$P2_1/n$	$P2_1/n$	$P2_1/n$	$P2_1/n$	$P2_1/n$
a (Å)	6.9177(10	6.9198(1)	6.9235(1)	6.9284(1)	6.9335(1)	6.9414(1)
b (Å)	9.8805(2)	9.9114(2)	9.9491(1)	9.9899(2)	10.0299(2)	10.0762(2)
c (Å)	7.1781(1)	7.1815(1)	7.1847(1)	7.1880(1)	7.1907(1)	7.1970(2)
β (deg)	98.4904(10)	98.4338(11)	98.3669(8)	98.2997(12)	98.2425(11)	98.1913(13)
V (Å^3)	485.25(1)	487.22(1)	489.63(1)	492.30(1)	494.89(1)	498.24(2)
Z	2	2	2	2	2	2
d_{calc} (g cm^{-3})	1.867	1.860	1.851	1.841	1.831	1.819
crystal size (mm)	sphere 0.30	sphere 0.30	sphere 0.30	sphere 0.30	sphere 0.30	sphere 0.30
F(000)	284	284	284	284	284	284
abs. coeff (mm^{-1})	2.02	2.02	2.01	1.99	1.98	1.97
2θ range (deg)	4.12−72.60	4.12−71.62	4.10−72.66	4.08−72.62	4.06−72.60	4.04−72.60
index ranges (h, k, l)	−11/11,−16/15, −11/11	−11/11,−16/15, −11/11	−11/11,−16/15, −11/11	−11/11,−16/15, −11/11	−11/11,−16/15, −11/11	−11/11,−16/15, −11/11
no. refl. collected	4604	4622	4621	4710	4713	4748
no. unique refl.	2450	2461	2488	2497	2502	2529
R equivalent refl.	0.011	0.011	0.013	0.012	0.015	0.017
data completeness	0.995	0.995	0.997	0.999	0.995	0.999
GOF[a] on F	1.98	1.99	1.99	1.95	1.99	1.97
no. refl. > 4$\sigma(I)$	1924	1885	1880	1774	1688	1577
R_1 [I > 4σ (I)][b]	0.0187	0.0195	0.0196	0.0213	0.0225	0.0232
wR_2 [I > 4$\sigma(I)$][c]	0.0200	0.0220	0.0200	0.0220	0.0240	0.0240
extinct. coefficient	4.62 × 10^{-6}	4.65 × 10^{-6}	5.00 × 10^{-6}	4.46 × 10^{-6}	4.83 × 10^{-6}	6.63 × 10^{-6}
largest diff. peak and hole (e Å^{-3})	0.48/−0.39	0.48/−0.39	0.45/−0.37	0.43/−0.32	0.38/−0.34	0.49/−0.32

[a] GOF = goodness-of-fit = $[\Sigma(|F_o| - |F_c|)^2/(m-p)]^{1/2}$ where m is the number of reflections and p the number of variables. [b] $R_1 = \Sigma||F_o| - |F_c||/\Sigma|F_o|$. [c] $wR_2 = [\Sigma w(|F_o| - |F_c|)^2/\Sigma w|F_o|^2]^{1/2}$, $w = 1/\sigma^2(F_o)$.

complex, the Cu−O(H_2O) bond lengthens by 3 units, that is, 0.219 Å, while the Cu−O(MeO) bond shortens by this amount, leading to the following estimated bond lengths:

$$\begin{aligned} &\text{Cu-O(carb)} \quad 1.955\ \text{Å} \\ &\text{Cu-O(MeO)} \quad 1.990\ \text{Å} \\ &\text{Cu-O}(H_2O) \quad 2.250\ \text{Å} \end{aligned} \tag{3}$$

Proportions of the Three Forms in Thermal Equilibrium. Electronic Spectrum. Numerous measurements were made on several crystals and various crystal faces, and these were found to be very similar; the spectrum of a typical crystal is shown in Figure 2. The results were reproducible and show just three peaks due to "d-d" transitions in the region 9000−20,000 cm^{-1}: at 13050 ($^2B_{2g}(xz)$, $^2B_{3g}(yz)$), 10250 ($^2B_{1g}(xy)$), and ∼7700 cm^{-1} ($^2A_g(z^2)$) at 15 K. (Here the symmetry designations of the excited states in the D_{2h} point group are given, together with the d-orbital(s) from which the electron is excited.) The peak energies are quite similar to those reported for the $[Cu(H_2O)_6]^{2+}$ ion in various lattices.[27] The splitting due to the orthorhombic component of the ligand field was not resolved. A weak high-energy shoulder reported by Hathaway et al.[20] was not observed.

The region 4600−5400 cm^{-1} exhibited an interesting additional feature shown magnified in Figure 2b. A peak at 5070 cm^{-1} progressively replaced a peak at 4870 cm^{-1} as the temperature was increased from 15 to 300 K. These peaks may be assigned to a combination band of the asymmetric stretching (ν_3) and bending (ν_2) vibrations of the water molecule[28] and the change suggests a profound alteration of the hydrogen-bonding interactions as the temperature rises. The observation of two infrared combination peaks at intermediate to high temperature suggests the existence of two distinct types of water molecules in this temperature range. The fact that the peak at 5070 cm^{-1} has almost replaced that at 4870 cm^{-1} by 300 K might seem inconsistent with the fact that the model assumes that only ∼35% of complexes have switched to a tetragonally compressed geometry at this temperature (see Table 5). However, this is not the case if the former peak is due to the water molecules of not only the compressed complexes but also their neighbors, as it is to these that the hydrogen bonding has been disrupted. The peak at 4870 cm^{-1} would then be due just to the water molecules in the small regions of the lattice in which thermal excitation has not occurred.

Angular Overlap Bonding Parameters of the Forms. Angular overlap metal−ligand bonding parameters were estimated for the tetragonally elongated complex present at low temperature by reproducing the observed transition energies and

dx.doi.org/10.1021/ic200554f |*Inorg. Chem.* 2011, 50, 4900–4916

Table 3. Cu−O Bond Lengths (Å) and Differences in Mean-Square Displacements between the Cu and O Ligand Atoms along the Directions of the Cu−O Bonds (Å^2) for *trans*-Diaquabis(methoxyacetato)copper(II)

	T = 90 K	T = 120 K	T = 140 K	T = 160 K	T = 180 K	T = 200 K	T = 220 K	T = 240 K
Cu−O(carb)	1.9552(6)	1.9541(6)	1.9523(6)	1.9508(6)	1.9486(6)	1.9463(7)	1.9430(7)	1.9390(7)
Cu−O(MeO)	2.2049(6)	2.2027(6)	2.2014(6)	2.1994(7)	2.1915 (7)	2.1873 (7)	2.1796(8)	2.1721(7)
Cu−O(H_2O)	2.0418(7)	2.0468(7)	2.0525(7)	2.0594(7)	2.0656(8)	2.0740(8)	2.0871(9)	2.1020(8)
Average Cu−O	2.067	2.068	2.069	2.070	2.069	2.069	2.070	2.071
ΔU_{obs}[Cu−O(carb)][a]	0.0021(2)	0.0024(2)	0.0024(2)	0.0026(2)	0.0024(2)	0.0023(2)	0.0025(3)	0.0025(2)
ΔU_{obs}[Cu−O(MeO)]	0.0017(2)	0.0020(2)	0.0021(2)	0.0028(2)	0.0037(2)	0.0042(3)	0.0051(3)	0.0062(3)
ΔU_{obs}[Cu−O(H_2O)]	0.0022(2)	0.0024(2)	0.0026(2)	0.0031(2)	0.0036(3)	0.0048(3)	0.0054(3)	0.0064(3)
	T = 260 K	T = 280 K	T = 298 K	T = 310 K	T = 320 K	T = 330 K	T = 340 K	T = 350 K
Cu−O(carb)	1.9368(8)	1.9331(8)	1.9308(8)	1.9298(8)	1.9285(9)	1.9273(11)	1.9271(11)	1.9266(14)
Cu−O(MeO)	2.1629(8)	2.1502(8)	2.1426(8)	2.1375(9)	2.1325(10)	2.1256(11)	2.1218(11)	2.1155(14)
Cu−O(H_2O)	2.1141(10)	2.1338(11)	2.1461(11)	2.1590(11)	2.1687(12)	2.1745(15)	2.1846(16)	2.1957(20)
Average Cu−O	2.071	2.072	2.073	2.075	2.077	2.076	2.078	2.079
ΔU_{obs}[Cu−O(carb)]	0.0023(3)	0.0021(3)	0.0025(3)	0.0024(3)	0.0021(4)	0.0018(5)	0.0018(5)	0.0003(7)
ΔU_{obs}[Cu−O(MeO)]	0.0072(3)	0.0080(3)	0.0088(3)	0.0092(4)	0.0094(4)	0.0088(5)	0.0091(5)	0.0085(7)
ΔU_{obs}[Cu−O(H_2O)]	0.0078(4)	0.0080(4)	0.0086(4)	0.0088(5)	0.0086(5)	0.0079(6)	0.0086(7)	0.0090(10)

[a] A reviewer expressed some concern about the accuracy of the ΔU_{obs}(M-O) values given in Tables 3 and 4 because of the particular weighting scheme chosen for least-squares refinements in this study. Distributions of $\langle w\Delta^2 \rangle$ ($\Delta = |F_o| - |F_c|$) against sin θ/λ, $|F_o|$and various classes of indices are routinely calculated and analyzed in the least-squares routine of *teXsan*;[25b] no unusual trends were detected for any structural refinements in this study. Furthermore, the sensitivity of ΔU_{obs}(M-O) values was checked by refining the 90 K-structure of [Cu(MeOAc)$_2$(H_2O)$_2$] using the Cruickshank,[a] three-term Chebyshev,[b] and Sheldrick[c] weighting schemes; the resulting ΔU_{obs}(Cu−O) values varied by no more than ±1 e.s.d from those determined using the weighting scheme in this study, $1/\sigma^2(F_o)$, and reported in these tables. [a]Cruickshank, D.W. J *Crystallographic Computing*. Copenhagen: Munksgaard, **1970**, p 195. [b]Carruthers, J. R.; Watkin, D. J. *Acta Crystallogr.* **1997**, *A35*, 698. [c]Sheldrick, G.M. *SHELXL97: Program for the Refinement of Crystal Structures*. University of Göttingen, Germany.

Table 4. Ni−O Bond Lengths (Å) and Differences in Mean-Square Displacements between the Ni and O Ligand Atoms along the Directions of the Ni−O Bonds (Å^2) for *trans*-Diaquabis(methoxyacetato)nickel(II)

	T = 100 K	T = 150 K	T = 200 K	T = 250 K	T = 300 K	T = 350 K
Ni−O(carb)	2.0249(5)	2.0253(6)	2.0235(6)	2.0227(7)	2.0207(8)	2.0207(8)
Ni−O(MeO)	2.0424(5)	2.0425(6)	2.0430(5)	2.0436(6)	2.0444(7)	2.0464(7)
Ni−O(H_2O)	2.0684(6)	2.0696(7)	2.0732(6)	2.0714(8)	2.0736(9)	2.0772(10)
average Ni−O	2.0452	2.0458	2.0466	2.0459	2.0462	2.0481
ΔU_{obs}[Ni−O(carb)]	0.0023(2)	0.0020(2)	0.0025(2)	0.0024(2)	0.0024(3)	0.0025(3)
ΔU_{obs}[Ni−O(MeO)]	0.0019(2)	0.0016(2)	0.0018(2)	0.0019(2)	0.0015(3)	0.0014(3)
ΔU_{obs}[Ni−O(H_2O)]	0.0013(2)	0.0010(2)	0.0010(2)	0.0005(3)	0.0004(3)	0.0005(4)

low temperature g-values using the computer program CAMMAG.[29] As an initial estimate, except for the π-parameter of carboxylate, the bonding parameters reported for water[30] were used, corrected for the different bond distances by assuming a $1/r^6$ dependence, as in previous studies.[31] For carboxylate, the out-of-plane π parameter was set to 0.25 e_σ, and the in-plane to half this value, as for similar ligands.[32] The parameters were then varied to produce optimum agreement with experiment. Only modest changes were required, the optimum values being

$$\text{O(carb)}\ e_\sigma = 5250,\ e_{\pi x} = 650,\ e_{\pi y} = 1310\ \text{cm}^{-1} \quad (4)$$

$$\text{O(MeO)}\ e_\sigma = 2100,\ e_{\pi x} = e_{\pi y} = 200\ \text{cm}^{-1}$$

$$\text{O(H}_2\text{O)}\ e_\sigma = 4300,\ e_{\pi x} = e_{\pi y} = 715\ \text{cm}^{-1}$$

The parameters are quite similar to those reported for other Cu(II) complexes.[30−33] The calculated transition energies, 13110, 12400 (13050), 10330 (10250), 7750 (~7700) cm^{-1}, are in good agreement with the experimental values observed at low temperature (shown in parentheses). Here, a correction of −2000 cm^{-1} was added to the lowest energy transition involving the d_{z^2} orbital to take account of d-s mixing, as in other similar systems.[33] The g-values calculated using an isotropic k value of 0.86 also agree well with those observed experimentally at low temperature,[22] these being shown in parentheses: 2.045 (2.045), 2.125 (2.126), 2.432 (2.432).

Correcting for the differences in bond length as given in eq 2, the bonding parameters for the complex with a compressed tetragonal geometry are estimated as

$$\text{O(carb)}\ e_\sigma = 6618,\ e_{\pi x} = 819,\ e_{\pi y} = 1651\ \text{cm}^{-1} \quad (5)$$

$$\text{O(MeO)}\ e_\sigma = 2576,\ e_{\pi x} = e_{\pi y} = 245\ \text{cm}^{-1}$$

$$\text{O(H}_2\text{O)}\ e_\sigma = 2827,\ e_{\pi x} = e_{\pi y} = 470\ \text{cm}^{-1}$$

dx.doi.org/10.1021/ic200554f |*Inorg. Chem.* 2011, 50, 4900–4916

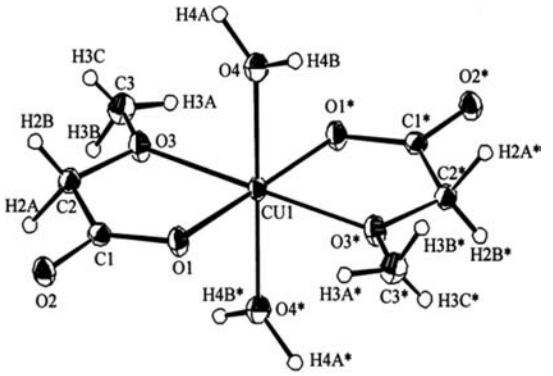

Figure 1. Molecular structure of *trans*-diaquabis(methoxyacetato)-copper(II), $[Cu(MeOAc)_2(H_2O)_2]$, determined at $T = 298$ K showing 20% probability ellipsoids. The copper and analogous nickel compound are isostructural and the metal ions are located at inversion centers; M-O(1) = M-O(carb); M-O(3) = M-O(MeO); M-O(4) = M-O(H_2O).

These were used to calculate the transition energies and *g*-values of the compressed tetragonal complex using CAMMAG. The calculated transition energies are: 13170, 12025 (12400), 9990 (~9500), 6085 (~7200) cm^{-1}. Here the transition energies have been corrected by -1500 cm^{-1} to allow for the energy shift of the d_{z^2} ground state orbital due to d-s mixing, it being assumed that the effect is slightly smaller than in the tetragonally elongated complex.[33] (The values in parentheses are the transition energies observed at room temperature.) It may be seen that the peaks due to the compressed complex, when added to those of the ~75% complexes remaining in the tetragonally elongated form, could well lie under the band envelope observed at high temperature, particularly when it is noted that the lowest energy peak is broad and partly masked by infrared overtones. The calculated *g*-values using the AOM parameters of the tetragonally compressed complex in eq 5 are 1.990, 2.261, and 2.366 assuming a *k* value of 0.86.

Calculation of the Proportion of the Complexes in each Form. Within the framework of the proposed model, the temperature dependence of the lowest *g*-value, g_1, is due solely to the thermal population of the tetragonally compressed state, so the proportion x in this form may easily be calculated. Accordingly, the experimental $g_1(T)$ value[22] at a given temperature T is given by

$$g_1(T) = 1.990x + 2.045(1 - x) \quad (6)$$

where 2.045 is the experimental value at 4.2 K; the calculated x values are given in Table 5.

Knowledge of the proportion with a compressed geometry, together with the estimate of the two higher *g*-values of the compressed form, 2.261 and 2.366, allows the upper *g*-values of the complexes remaining in the tetragonally elongated form, g_{2elong} and g_{3elong}, to be calculated from analogous equations:

$$g_2(T) = 2.261x + g_{2elong}(1 - x) \quad (7)$$

$$g_3(T) = 2.366x + g_{3elong}(1 - x) \quad (8)$$

where $g_2(T)$ and $g_3(T)$ are experimental values.[22] The g_{2elong} and g_{3elong} values given in Table 5 show a marked temperature dependence, converging at high temperature. This suggests that the tetragonally elongated complexes undergo an SG-type

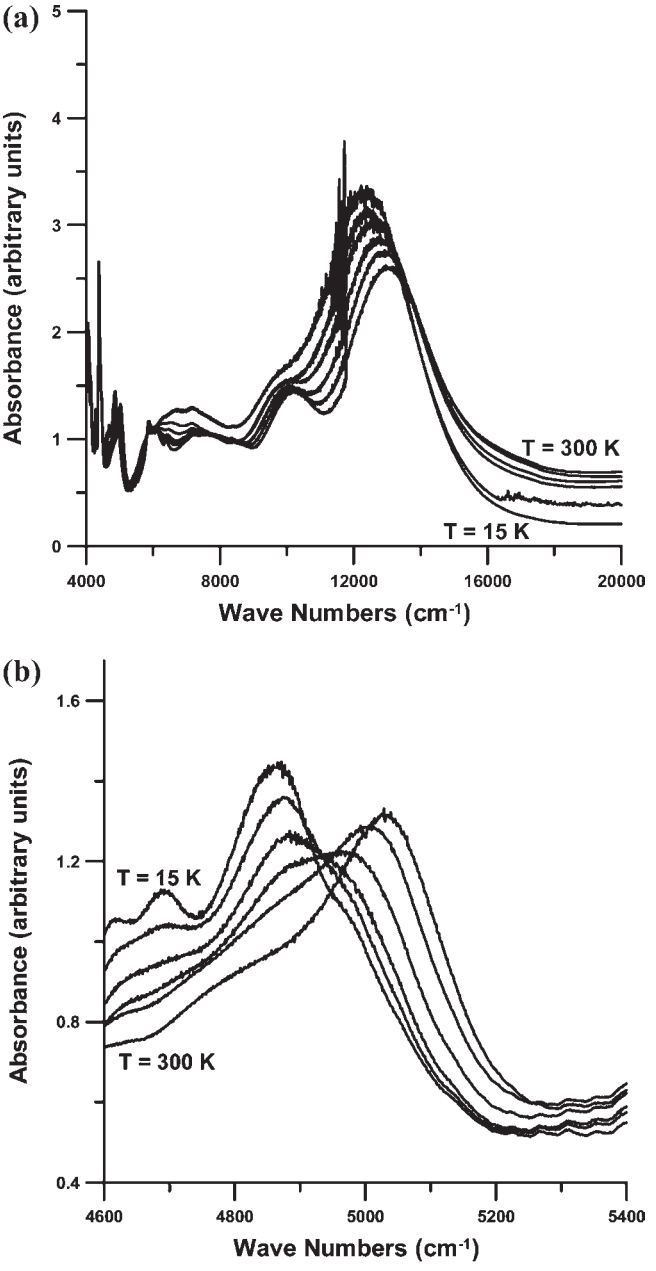

Figure 2. (a) Single-crystal electronic spectrum of $[Cu(MeOAc)_2(H_2O)_2]$ from 15 to 300 K in the visible and (b) NIR regions.

equilibrium of the kind shown by many other Cu(II) complexes, the two longer bond lengths and their associated *g*-values being interchanged in the higher-energy state. The shift in each *g*-value may be used to estimate the proportion y of the tetragonally elongated complexes that have been thermally excited in the SG equilibrium at each temperature:

$$g_{2elong} = 2.126(1 - y_2) + 2.432y_2 \quad (9)$$

$$g_{3elong} = 2.432(1 - y_3) + 2.126y_3 \quad (10)$$

where 2.126 and 2.432 are observed values at 4.2 K;[22] calculated *y*-values are given in Table 5, and it is pleasing that both g_{elong} values give similar estimates of y within the SG model, and the

dx.doi.org/10.1021/ic200554f |*Inorg. Chem.* 2011, 50, 4900–4916

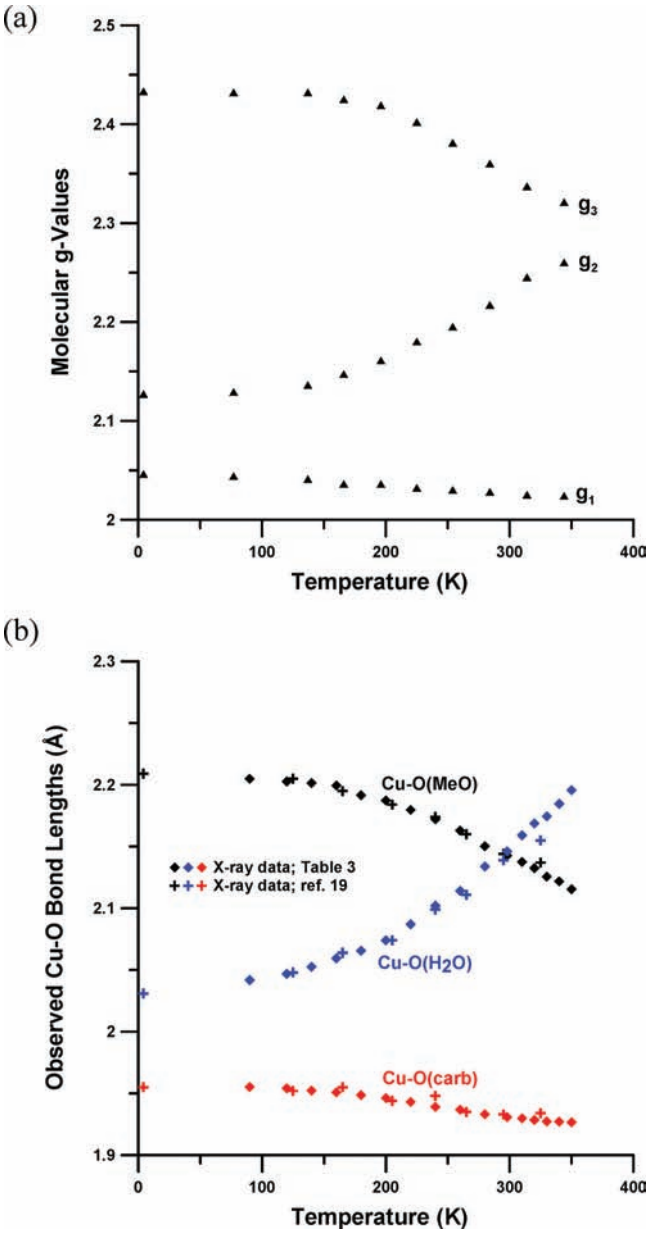

Figure 3. Plots of (a) molecular *g*-values[22] and (b) Cu−O bond lengths as a function of temperature for $[Cu(MeOAc)_2(H_2O)_2]$.

average value y_{ave} was used in subsequent calculations. Substituting these equations into eqs 7 and 8 gives the final expressions for $g_2(T)$ and $g_3(T)$:

$$g_2(T) = 2.261x + 2.126(1-x)(1-y_2) + 2.432(1-x)y_2 \quad (11)$$

$$g_3(T) = 2.366x + 2.432(1-x)(1-y_3) + 2.126(1-x)y_3 \quad (12)$$

Temperature Dependence of the Observed Bond Lengths. Knowledge of the fractional occupancy of the three different complexes in thermal equilibrium at each temperature, plus estimates of their bond lengths, makes it straightforward to

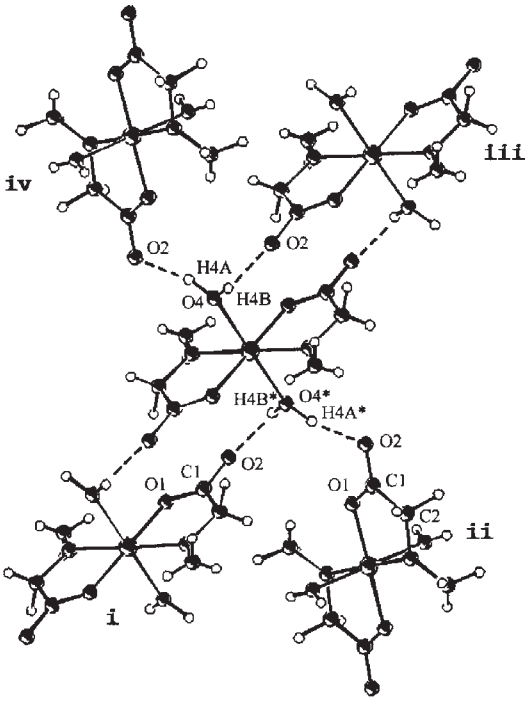

Figure 4. ORTEP drawing showing hydrogen-bonding contacts between coordinated waters of central $[Cu(MeOAc)_2(H_2O)_2]$ complex O4 (x, y, z) and carbonyl oxygen atoms $O2^{iii}$ ($-1+x$, y, z) and $O2^{iv}$ ($-1/2+x$, $1/2-y$, $1/2+z$), and O4* ($-x$, $-y$, $-z$) and carbonyl oxygen atoms $O2^{i}$ ($1-x$, $-y$, $-z$) and $O2^{ii}$ ($1/2-x$, $-1/2+y$, $-1/2-z$) of four adjacent complexes; 10% probability ellipsoids are drawn. Two other adjacent complexes having O2 (x, y, z) and $O4^{v}$ ($1/2+x$, $1/2-y$, $-1/2+z$) and O2* ($-x$, $-y$, $-z$) and $O4^{vi}$ contacts ($-1/2-x$, $-1/2+y$, $1/2-z$,) are not shown for purposes of clarity.

calculate the average bond lengths (Å) at each temperature:

$$\begin{aligned} \text{Cu-O(carb)} &= 1.882x + 1.955(1-x)(1-y_{ave}) \\ &\quad + 1.955(1-x)y_{ave} \\ &= 1.882x + 1.955(1-x) \end{aligned} \quad (13)$$

$$\begin{aligned} \text{Cu-O(MeO)} &= 2.136x + 2.209(1-x)(1-y_{ave}) \\ &\quad + 1.990(1-x)y_{ave} \end{aligned} \quad (14)$$

$$\begin{aligned} \text{Cu-O}(H_2O) &= 2.177x + 2.031(1-x)(1-y_{ave}) \\ &\quad + 2.250(1-x)y_{ave} \end{aligned} \quad (15)$$

The calculated Cu−O bond lengths are given in Table 5 and are compared with experiment in Figure 5. Agreement is excellent for the Cu−O(carb) and Cu−O(MeO) bonds, but the Cu−$O(H_2O)$ bond length is underestimated, especially at higher temperatures. However, a further effect that should be included is any underlying variation of bond length with temperature. An independent indication of this is given by the behavior of the analogous Ni(II) complex. Here, the average Ni−O distance increases slightly (~0.003 Å) on going from 100 to 350 K (see Table 4), with this increase being entirely because of a significant expansion of the Ni−$O(H_2O)$ distance which increases by ~0.01 Å (see Table 4). If it is assumed that the increase in the average Cu−O bond length is due entirely to an underlying increase in the Cu−$O(H_2O)$ distance, then the calculated values can be corrected by the following equation: $Cu-O(H_2O)_{corr}$

dx.doi.org/10.1021/ic200554f |*Inorg. Chem.* 2011, 50, 4900–4916

Table 5. Calculated x and y Values, $g_{2,3elong}$ Values, and Cu−O Bond Lengths As a Function of Temperature

T (K)	x^a	$g_{2elong}{}^b$	$g_{3elong}{}^b$	$y_2{}^c$	$y_3{}^c$	y_{ave}	Cu−O(carb)^d	Cu−O(MeO)^d	Cu−O(H_2O)$_{uncorr}{}^d$	Cu−O(H_2O)$_{corr}{}^e$
4.2	0.0	2.126	2.432	0.0	0.0	0.0	1.955	2.209	2.031	2.031
77	0.0364	2.123	2.433	−0.0099	−0.0048	−0.0073	1.952	2.206	2.036	2.038
137	0.0909	2.122	2.438	−0.0117	−0.0181	−0.0149	1.948	2.202	2.044	2.049
166	0.182	2.120	2.437	−0.0181	−0.0162	−0.0171	1.942	2.196	2.058	2.065
196	0.182	2.138	2.430	0.0378	0.0078	0.0228	1.942	2.192	2.062	2.072
225	0.255	2.151	2.413	0.0818	0.0619	0.0719	1.936	2.179	2.080	2.094
254	0.291	2.167	2.386	0.133	0.151	0.142	1.934	2.166	2.095	2.113
284	0.327	2.194	2.356	0.223	0.249	0.236	1.931	2.150	2.114	2.135
314	0.382	2.234	2.318	0.352	0.374	0.363	1.927	2.132	2.136	2.163
344	0.400	2.258	2.290	0.431	0.466	0.448	1.926	2.121	2.148	2.180

[a] Proportion of compressed complexes (x) calculated using eq 6; see text. [b] g-values for complexes in tetragonally elongated form calculated using eqs 7 and 8. [c] y-values calculated using eqs 9 and 10; negative values considered to be zero for calculational purposes. [d] Cu−O bond lengths calculated using eqs 13−15. [e] Cu−O(H_2O) bond lengths corrected for lattice expansion: Cu−O(H_2O)$_{corr}$ (Å) = Cu−O(H_2O)$_{uncorr}$ + $3(9.0199 \times 10^{-8})T^2$; see text.

(Å) = Cu−O(H_2O)$_{uncorr}$ + $3(9.0199 \times 10^{-8})T^2$. (A plot of the average Cu−O bond length with temperature is given as Supporting Information (S-3)). The corrected and uncorrected Cu−O(H_2O) bond lengths are shown in Figure 5 and agreement with experiment is now excellent. In particular, the Cu−O(H_2O) and Cu−O(MeO) bond lengths now cross at ∼295 K, as observed experimentally (see Table 3).

An independent check that the model is realistic may be obtained by estimating the parameters x and y using the observed changes in bond lengths rather than g-values, as in the above method. The x and y values estimated in this way at the temperatures of the structure determinations are given in Table 6 (the bond to water was not included as the bond length of the lowest energy form apparently varies with temperature). It is seen that the results are broadly similar to those obtained using the g-values except at low temperatures, where the latter values are lower, even falling to zero or below. The estimate of y derived from the upper two g-values may well be less reliable than those from bond lengths as their derivation relies on the accuracy of the AOM calculation of the two higher g-values of the compressed complex. (Note: a similar argument does not apply to the population of the compressed form of the complex, x, which depends solely on the estimate of the lowest g-value of the compressed complex, which is quite insensititve to the AOM calculation.) According to eqs 13−15, the proportion of structures (P) associated with the lower- and higher-energy states of the tetragonally elongated form are $1 - (x + y) + xy$ and $y - xy$, respectively, and the proportion of compressed structures is x. The variation of these proportions with temperature estimated using all the experimental data in Table 6 is shown in Figure 6. The best-fit curves of the form $P = a + bT^2 + cT^3 + dT^4$, where T is temperature and a, b, c, d are constants, are shown for each of the three forms. It is seen that the proportion of the compressed form rises progressively to ∼39% as the temperature approaches 358 K, at which temperature the proportions of the tetragonally elongated "unswitched" and "switched" forms are equal (∼30%). The fact that the different sets of experimental data yield similar proportions suggests that the proposed model does provide a realistic picture of the thermal behavior of the compound, at least in a broad sense.

Temperature Dependence of the Thermal Ellipsoid Parameters. The difference displacement parameters between pairs of atoms, ΔU,[34] is a way of quantifying Jahn−Teller distortions[35,36] when taken between the metal and ligand atoms

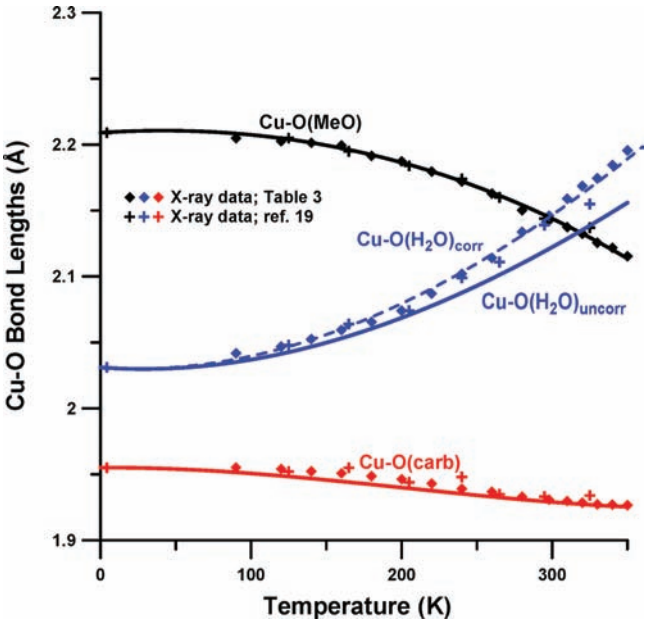

Figure 5. Experimental Cu−O bond lengths and curves fitted with Cu−O bond lengths calculated using x and y_{ave} values in Table 5 and eqs 13−15. The calculated, or uncorrected Cu−O(H_2O)$_2$ bond lengths (solid blue curve), have been corrected (dashed blue curve) according to the equation: Cu−O(H_2O)$_{corr}$ = Cu−O(H_2O)$_{uncorr}$ + $3(9.0199 \times 10^{-8})T^2$; see text.

along the direction of the metal−ligand bond. The observed quantity, ΔU_{obs}, will be the sum of the usual small amplitude atomic displacement due to bond stretching motions, $\langle \Delta U_{str} \rangle$, and to the large amplitude displacements of different conformers, ΔU_{dis}:[35]

$$\Delta U_{obs} = \Delta U_{dis} + \langle \Delta U_{str} \rangle \qquad (16)$$

The ΔU_{obs} for the Ni−O bonds in the [Ni(MeOAc)$_2$(H_2O)$_2$] complex shows very little temperature dependence; see Table 4. The thermal ellipsoids themselves show the usual temperature dependence, but as most of this is due to the correlated motion of the low-energy acoustic vibrational modes of the crystal, the contribution of $\langle \Delta U_{str} \rangle$ is small and ΔU_{obs} is only slightly temperature dependent. The ΔU_{obs} values for [Cu(MeOAc)$_2$(H_2O)$_2$], shown in Figure 7 and given in Table 3, however, have a much larger

dx.doi.org/10.1021/ic200554f |Inorg. Chem. 2011, 50, 4900–4916

Table 6. Calculated x and y Values As a Function of Temperature

T (K)	x determined from EPR g-values[a]	y_{ave} determined from EPR g-values[a]	x determined from Cu−O bond lengths[b]	y determined from Cu−O bond lengths[c]	x determined from Cu−O bond lengths[d]	y determined from Cu−O bond lengths[e]
4.2	0.0	0.0			0.0	0.0
77	0.0364	−0.0073 = 0.00				
90			0.00	0.0196		
120			0.0123	0.0250		
125					0.0411	0.0048
137	0.0909	−0.0149 = 0.00				
140			0.0370	0.0232		
160			0.0575	0.0262		
165					0.0	0.0639
166	0.182	−0.0171 = 0.00				
180			0.0877	0.0556		
196	0.182	0.0228				
200			0.119	0.0674		
205					0.151	0.0753
220			0.164	0.0951		
225	0.255	0.0719				
240			0.219	0.122	0.096	0.141
240						
254	0.291	0.142				
260			0.249	0.170		
265					0.274	0.182
280			0.300	0.241		
284	0.327	0.236				
295					0.301	0.281
298			0.332	0.288		
310			0.345	0.323		
314	0.382	0.363				
320			0.363	0.358		
325					0.288	0.327
330			0.380	0.410		
340			0.382	0.438		
344	0.400	0.448				
350			0.389	0.487		

[a] See Table 5. [b] Determined using eq 13) and Cu−O bond lengths given in Table 3. [c] Determined using eq 14 and Cu−O bond lengths given in Table 3. [d] Determined using eq 13 and Cu−O bond lengths from ref 19. [e] Determined using eq 14 and Cu−O bond lengths from ref 19.

temperature dependence compared to the Ni(II) complex, with the ΔU_{obs} values for the Cu−O(MeO) and Cu−O(H_2O) bonds much larger than those for Cu−O(carb). This is due to the large ΔU_{dis} contribution that is given by[35]

$$\Delta U_{dis} = (\Delta d)^2 - \langle \Delta d \rangle^2 \qquad (17)$$

where $\Delta d = 1/2(r_1 - r_2)$ is half the difference of the actual (static) bond lengths, and $\langle \Delta d \rangle = 1/2(\langle r_1 \rangle - \langle r_2 \rangle)$ is half the difference of the observed bond lengths for two conformers with the bond lengths r_1 and r_2 interchanged. A plot of ΔU_{dis} versus $\langle \Delta d \rangle$ leads to an inverted parabola.[35]

The experimental ΔU_{obs} values for $[Cu(MeOAc)_2(H_2O)_2]$ differ from those of the $(ND_4)_2[Cu(D_2O)_6](SO_4)_2$ Tutton salt in a number of ways.[36] For example, the two bonds with the strongly temperature dependent ΔU_{obs} values are clearly different from each other, as expected because of the chemical inequivalency of the Cu−O(MeO) and Cu−O(H_2O) bonds, in contrast to the ΔU_{obs} values observed for the chemically equivalent Cu−O(7) and Cu−O(8) bonds in the Tutton salt, which are nearly identical from 90 to 320 K.[14] Interestingly, as the temperature increases, the values of ΔU_{obs}[Cu−O(MeO)] and ΔU_{obs}[Cu−O(H_2O)] for $[Cu(MeOAc)_2(H_2O)_2]$ go through a maximum and start to decrease at higher temperature, in stark contrast to the steadily increasing ΔU_{obs} values observed for the Cu−O(7) and Cu−O(8) bonds in the Tutton salt.

In the present case, eq 16 cannot be used, as the different conformers are not a simple interchange of bond lengths. Analogous to eqs 13−15, the temperature dependent ΔU_{obs} values (Å^2) can be written as[35]

$$\begin{aligned}\Delta U_{obs}[\text{Cu-O(carb)}] &= \{1.882 - [\text{Cu-O(carb)}]\}^2 x \\ &+ \{1.955 - [\text{Cu-O(carb)}]\}^2 (1-x)(1-y) \\ &+ \{1.955 - [\text{Cu-O(carb)}]\}^2 (1-x)y + \langle \Delta U_{str} \rangle \\ &= \{1.882 - [\text{Cu-O(carb)}]\}^2 x \\ &+ \{1.955 - [\text{Cu-O(carb)}]\}^2 (1-x) + \langle \Delta U_{str} \rangle \qquad (18)\end{aligned}$$

dx.doi.org/10.1021/ic200554f |Inorg. Chem. 2011, 50, 4900–4916

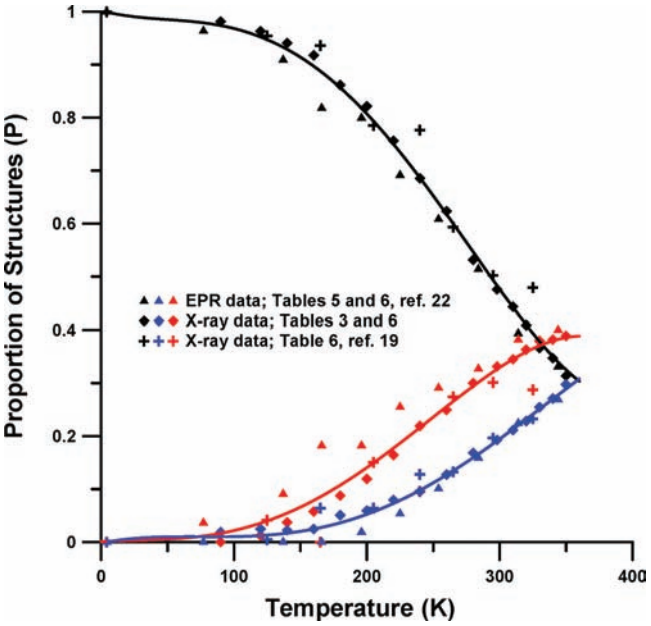

Figure 6. Proportions (P) of the three structural forms as a function of temperature determined using the x and y values given in Table 6. The proportion of structures associated with the lowest-energy minimum is shown by the black curve, the "flipped" structures by the blue curve, and the compressed structures by the red curve. Notice that the curves representing the two tetragonally elongated structures (black and blue curves) intersect at 358 K, the temperature at which the two minima switch; see text.

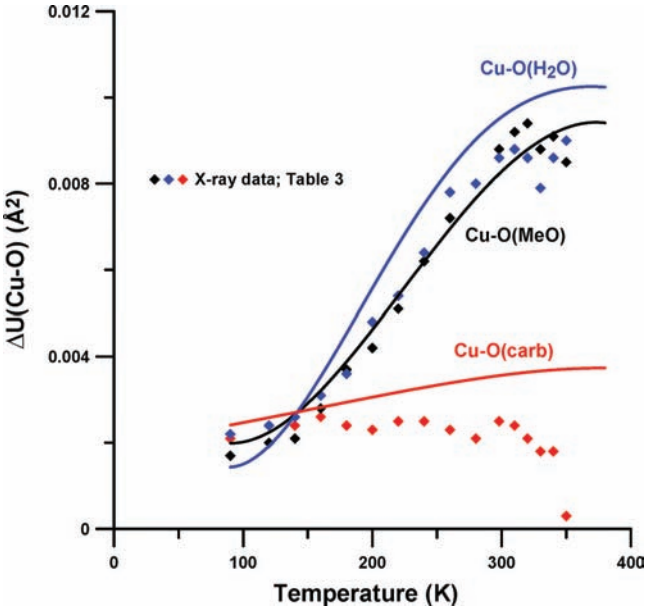

Figure 7. Plots of ΔU(Cu−O) as a function of temperature; the colored diamonds represent the experimental values given in Table 3, whereas the values of Prout et al.[19] have not been included as they show a very large scatter. The curves were fitted to ΔU(Cu−O) values calculated with eqs 18−20 using the observed Cu−O bond lengths given in Table 3 and ref 19 and the best-fit with temperature values of x and y given in Table 6.

$$\Delta U_{obs}[\text{Cu-O(MeO)}] = \{2.136 - [\text{Cu-O(MeO)}]\}^2 x + \{2.209 - [\text{Cu-O(MeO)}]\}^2 (1-x)(1-y) + \{1.990 - [\text{Cu-O(MeO)}]\}^2 (1-x)y + \langle \Delta U_{str} \rangle \quad (19)$$

$$\Delta U_{obs}[\text{Cu-O(H}_2\text{O)}] = \{2.177 - [\text{Cu-O(H}_2\text{O)}]\}^2 x + \{2.031 - [\text{Cu-O(H}_2\text{O)}]\}^2 (1-x)(1-y) + \{2.250 - [\text{Cu-O(H}_2\text{O)}]\}^2 (1-x)y + \langle \Delta U_{str} \rangle \quad (20)$$

where Cu−O(carb), Cu−O(MeO), and Cu−O(H_2O) are the observed temperature dependent bond lengths. Equations 18−20 are evaluated using the best-fit with temperature x and y values given in Table 6 and the observed Cu−O bond lengths given in Table 3 and ref 19. To these calculated values are added the values $\langle \Delta U_{str} \rangle$ = 0.0024, 0.0017, and 0.0008 Å^2 for the Cu−O(carb), Cu−O(MeO), and Cu−O(H_2O) bonds, respectively, for mean-squared values due to bond stretching motions as observed for the isostructural $[Ni(MeOAc)_2(H_2O)_2]$ complex; see Table 4. Calculated ΔU_{obs} values are plotted as solid curves in Figure 7 along with the experimental values.

The agreement between the experimental ΔU_{obs} values and those calculated from eqs 18−20 is reasonable, capturing the main features. The calculated ΔU[Cu−O(carb)] values suggest a slight monotonic increase with increasing temperature, whereas a slight decrease is actually observed. The calculated ΔU[Cu−O(MeO)] and ΔU[Cu−O(H_2O)] values both peak at about 360 K, which is very close to what is observed. Interestingly, the presence of the maxima indicates that the energies of the two lowest-energy minima are approaching each other with increasing temperature and, in theory, should become equal at the temperature corresponding to the maxima.

As noted previously, the ΔU values for the Cu−O bonds in the $(ND_4)_2[Cu(D_2O)_6](SO_4)_2$ Tutton salt have been determined using high-precision X-ray diffraction data.[14a,15,36] The ΔU_{obs} values for Cu−O(7) and Cu−O(8) are both 0.020 Å^2 at 320 K, 5 °C below the decomposition temperature of the crystal. Assuming a simple SG-type equilibrium between these two elongated forms (no compressed structure, x = 0), eq 20 with Cu−O(8) − Cu−O(7) = Δd(Cu−O) = 0.291 Å (at 8 K)[14b] gives a maximum ΔU(Cu−O) value of 0.022 Å^2, slightly greater than observed as expected. However, a similar calculation for the Cu−O(MeO) and Cu−O(H_2O) bonds of $[Cu(MeOAc)_2(H_2O)_2]$ with Δd(Cu−O) = 0.219 Å (eqs 14 and 15) gives ΔU(Cu−O) = 0.013 Å^2, almost one-and-a-half times greater than the observed maximum of 0.0094(4) Å^2 (see Table 3). This is yet another indication that a compressed structure is being populated, as the sum of the proportions of the two orthorhombically distorted, tetragonally elongated complexes will now no longer be equal to one as required by the two-minima SG model.

Temperature Dependence of the XAFS. The k^2 weighted raw XAFS spectra together with their Fourier transform are given in Supporting Information for both the Ni(II) and Cu(II) complexes for a number of temperatures. The spectra have been analyzed using the Athena and Artemis software packages.[37] The spectra of the Ni(II) complex can be fitted using a model consisting of the atomic positions from the crystal structure together with temperature dependent Debye−Waller factors. Only small shifts of the positions consistent with a thermal contraction of the lattice were required. A similar approach with the Cu(II) complex was unsuccessful as may be expected from the observed temperature dependent bond lengths from the

dx.doi.org/10.1021/ic200554f |Inorg. Chem. 2011, 50, 4900–4916

crystal structure. Although it is not possible to fit the model proposed here involving the temperature dependent population of three different Cu(II) conformers because of the large number of adjustable parameters, there are subtle differences between the Ni(II) and Cu(II) XAFS that are consistent with this model.

At low temperature there are three different Cu−O bond lengths that will contribute to the major peak in R space, while at higher temperature there are nine different Cu−O bond lengths that will contribute. The population of these as the temperature is raised will tend to decrease the intensity of this peak faster than the Ni(II) complex, as is observed. The XAFS of the Ni(II) complex in k space shows the typical decrease in amplitude with increasing temperature, while that of the Cu(II) complex shows small changes in the range $k = 5-10$. There are also small shifts in the higher peaks of $|\chi(R)|$ that are more evident when the real and imaginary parts of $\chi(R)$ are plotted.

Thermal Behavior of the Tetragonally Elongated Complexes. The above simple model assumes that the convergence at high temperature of the higher two g-values of the tetragonally elongated complexes is caused by the thermal population of an upper state in which the lengths of the bonds to the methoxy and water ligands are interchanged, that is, that this set of complexes undergoes a SG-type equilibrium. Behavior of this kind has been observed for many other Cu(II) complexes.[2,6] In their original study,[7] Silver and Getz assumed Boltzmann statistics, with the shift at temperature T of the two higher g-factors from their low temperature values being given by

$$g_2(T) = g_2(\text{low temperature})K/(1+K) + g_3(\text{low temperature})/(1+K) \quad (21)$$

$$g_3(T) = g_3(\text{low temperature})K/(1+K) + g_2(\text{low temperature})/(1+K) \quad (22)$$

where $K = n_1/n_2 = \exp(\Delta E/kT)$, $\Delta E = E_2 - E_1$ is the energy difference between the two states, and each g-value is the average of the two levels weighted by its fractional population. For Cu^{2+} doped $K_2[Zn(H_2O)_6](SO_4)_2$, ΔE was found to be nearly temperature independent,[7] and the same has been found to be true for several other compounds. Occasionally, however, the data suggest that ΔE decreases as the temperature rises, this being ascribed to changes in the strain due to cooperative interactions between neighboring complexes[15] or lattice effects.[38]

The temperature dependence of the upper two g-values of the tetragonally elongated $[Cu(MeOAc)_2(H_2O)_2]$ molecules, g_{2elong} and g_{3elong} in Table 5, deviates significantly from the SG model in the above simple form. The g-values start to converge at ∼175 K (see Figure 8), corresponding to an energy $\Delta E = \sim 500\ cm^{-1}$ for the upper state using eqs 21−22. However, as the temperature rises, the convergence is more rapid than predicted by this equation, and by 300 K the g-values correspond to an energy separation $\Delta E = \sim 75\ cm^{-1}$. Better agreement is obtained assuming that ΔE decreases linearly as the temperature rises, as done previously to interpret the thermal behavior of the EPR spectrum of Cu^{2+} doped $Cs_2[Zn(H_2O)_6](ZrF_6)_2$,[38] although there is still some deviation of the g-values from the calculated curves. Note that when the simple SG model is extended in this way, it predicts that the upper two g-values actually cross at ∼358 K. The inversion of the two energy levels above this temperature is caused by the water becoming a weaker σ-donor than the methoxy ligand. Such behavior is also suggested by the dependence of the proportions of structures associated with the lower- and higher-energy states of

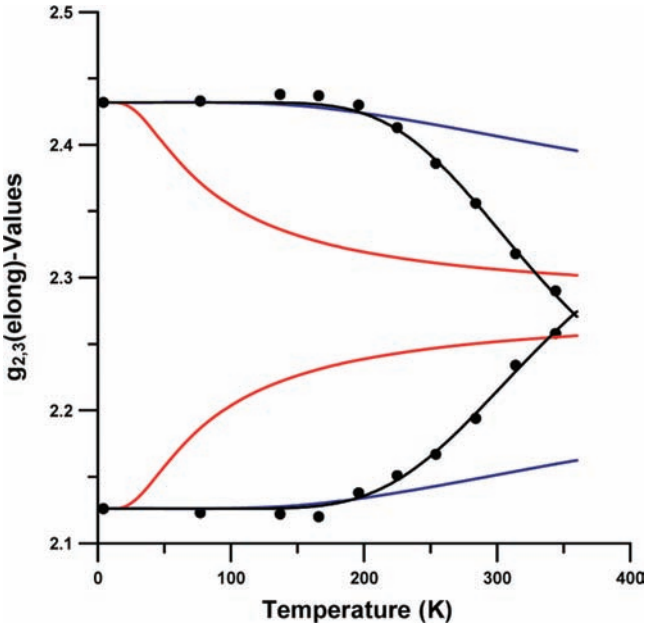

Figure 8. Upper two g_{elong}-values (shown as black circles) calculated for the tetragonally elongated forms of $[Cu(MeOAc)_2(H_2O)_2]$ using eqs 7 and 8, incorporating x values given in Table 5 and g-values from ref 22. The calculated temperature dependence assuming a SG-type thermal equilibrium using values of $\Delta E = 500\ cm^{-1}$ (blue curves), $75\ cm^{-1}$ (red curves), and with ΔE varying as a linear function of temperature (black curves) are shown; see eqs 21−22. Notice that the black curves intersect at 358 K.

the tetragonally elongated forms upon increasing temperature (see Figure 6), which intersect at the same temperature, 358 K.

The value of $\Delta E = \sim 500\ cm^{-1}$ at low temperature derived from the above analysis seems reasonable, as it is similar to, though somewhat larger than, the estimate of the orthorhombic component of the strain, $\sim 300\ cm^{-1}$, deduced from the EPR spectrum of Cu^{2+} doped into $[M(MeOAc)_2(H_2O)_2]$, M = Mg and Cd.[39] Estimates of the energy separation obtained using a SG-type analysis are typically 20−50% higher than the orthorhombic strain parameter, S_ε, derived using a JT vibronic coupling model.[8,10] For these doped systems, the curves calculated for the thermal behavior of the g-values agree quite well with experiment assuming that ΔE does not vary significantly with temperature. In considering the apparent temperature dependence of ΔE for the tetragonally elongated molecules in pure $[Cu(MeOAc)_2(H_2O)_2]$, it should be noted that the average Cu−O bond length increases as the temperature rises, and the present model ascribes this to a lengthening of the Cu−O(H_2O) bond. An increase in bond length to each water molecule will decrease its ligand−field strength, making it more similar to that of the methoxy group and energetically easier to switch the long and intermediate bond directions, resulting in a lower value of ΔE. The average Cu−O bond distance rises by ∼0.012 Å on going from 4.2 to ∼358 K, implying an increase of ∼0.036 Å in each Cu−O(H_2O) bond length. Both theory and experiment suggest that the σ-bonding strength of a ligand depends inversely on about the sixth power of the bond distance.[31] A bond length increase of ∼0.036 Å thus implies that e_σ drops from $4300\ cm^{-1}$ to $\sim 3800\ cm^{-1}$, a decrease of $\sim 420\ cm^{-1}$. This represents the contribution of the inequivalence of the ligands to the orthorhombic component of the strain,[9] which is the basic cause of the energy separation ΔE

between the two forms in the SG model.[7] Agreement with the estimate of ~425 cm^{-1} for the drop in ΔE derived from the SG analysis is thus good.

While the above treatment provides a reasonable explanation of the thermal behavior of the *g*-values of the set of complexes having a tetragonally elongated geometry, it must be recognized that it is quite simplistic. The present compound is more complicated than others to which the SG model has been applied. As discussed above, the basic metal−ligand bond lengths change slightly as the temperature rises. Moreover, the development of a population of complexes with a compressed tetragonal geometry may well influence the stereochemistry of the remaining complexes. Both of these factors are not included in the SG model in its simple form, which assumes that the upper state has bond lengths and *g*-values that are simply reversed in direction compared with those observed at low temperature. However, in our view, the current experimental data do not warrant a more detailed quantitative consideration; it must simply be recognized that the present treatment can be expected to provide only a general picture of what is occurring.

Vibronic Coupling Model and the Potential Surfaces of the Complexes. It is of interest to consider the potential surfaces of the different complexes present in $[Cu(MeOAc)_2(H_2O)_2]$ at low and high temperatures. A model has been developed to derive such a surface, and this has been applied to a wide range of complexes exhibiting temperature dependent crystal structures and/or *g*-values.[5,8−10,38] This model assumes that the basic "warped Mexican hat" potential surface is formed by the Jahn−Teller coupling of the E_g electronic state of the parent octahedral complex with the Jahn−Teller active e_g vibration.[1] The distortion is driven by the linear coupling constant A_1, but higher-order effects, represented by the parameter A_2, cause a "warping" of the potential surface. For six chemically identical ligands three equivalent minima occur, corresponding to tetragonal elongations with $d_{x^2-y^2}$-type ground states. The extent of the warping is normally expressed by the parameter β [$\sim A_2(A_1/h\nu_{JT})^2$], where ν_{JT} is the frequency of the e_g vibration. The magnitude of this parameter β indicates the natural tendency of the complex to adopt the tetragonally elongated form of the JT distortion.

For a complex formed by inequivalent ligands, such as the present one, the difference in σ-bonding strength imposes a "strain" upon the metal ion. Moreover, any anisotropy in the interactions with the surrounding lattice will add to this. The overall result is that the three minima in the potential surface are shifted from the positions corresponding to distortions of tetragonal symmetry and are no longer equal in energy. These effects are included by axial and orthorhombic strain parameters S_θ and S_ε, respectively. The approximation is made here that the strain term does not destroy the symmetry of the cubic part of the Hamiltonian.

The dynamic behavior of a complex of this kind is perhaps best understood by considering a circular section of the potential surface showing the way in which the energy changes as the ligands move along the normal coordinates of the e_g vibration, the position conventionally being defined by the angle φ.[1,8] The circular function is calculated at a constant Jahn−Teller radius, $\rho_m = A_1/K_2$, that of the complex at its energy minimum. A plot of this kind for the $[Cu(MeOAc)_2(H_2O)_2]$ complex at low temperature is shown as the red curve in Figure 9. For the calculation, the first and second order JT coupling constants were taken to be $A_1 = 800$ cm^{-1} and $A_2 = 11$ cm^{-1}, the wavenumber of the JT active

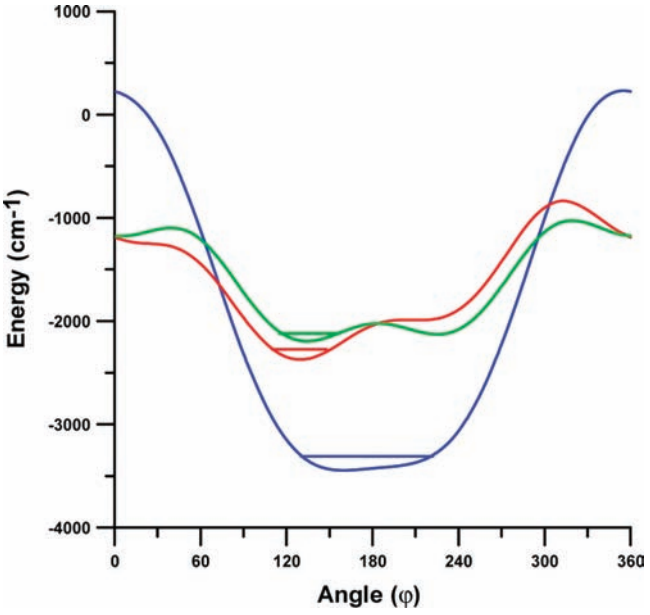

Figure 9. Plot of the lower potential energy surface of constant JT radius ($\rho_m = A_1/K_2$) for the tetragonally elongated and compressed structures of $[Cu(MeOAc)_2(H_2O)_2]$. The red curve corresponds to the low temperature tetragonally elongated structure determined using A_1 = 800 cm^{-1}, A_2 = 11 cm^{-1} (β = 175 cm^{-1}), $S_\theta = -600$ cm^{-1}, and S_ε = 300 cm^{-1}; the green curve corresponds to the high temperature elongated structure using the same parameters except S_ε = 50 cm^{-1}. The blue curve represents the energy of the compressed structure determined using the same A_1 and A_2 values but with $S_\theta = -2000$ cm^{-1} and S_ε = 100 cm^{-1}. It is assumed that the wavenumber of the JT active e_g vibrational mode (K_2) is 200 cm^{-1} for all structures.

e_g vibrational mode $K_2 = 200$ cm^{-1} ($\beta = \sim 175$ cm^{-1}) and the axial and orthorhombic components of the strain $S_\theta = -600$ cm^{-1} and $S_\varepsilon = 300$ cm^{-1}. These values are similar to those used to calculate the potential surface of the $[Cu(MeOAc)_2(H_2O)_2]$ complex in Cu^{2+} doped into $[M(MeOAc)_2(H_2O)_2]$, M = Mg and Cd[39] and the $[Cu(H_2O)_6]^{2+}$ ion.[8,38]

The minimum of the potential surface occurs close to the value of 120° which corresponds to a tetragonally elongated distortion along one of the three Cartesian axes of an octahedral complex.[1] A ligand field splitting Δ = 13050 cm^{-1} was used in the calculation, consistent with the observed optical spectrum. Higher-energy minima occur close to 240 and 0°, these corresponding to distortions in which the elongation occurs to the water and carboxylate ligands, respectively. The temperature dependence of the bond lengths and analysis of the *g*-values suggest that the orthorhombic component of the strain decreases as the temperature rises. The values g_1 = 2.056, g_2 = 2.116, g_3 = 2.439 calculated for the lowest vibronic energy level using an isotropic orbital reduction parameter k = 0.86 are similar to those observed experimentally at low temperature (g_1 = 2.045, g_2 = 2.126, g_3 = 2.432).[22] The angular form of the potential surface calculated using identical parameters but with the orthorhombic component of the strain S_ε reduced to 50 cm^{-1} is shown by the green line in Figure 9. The curve is similar to that of the complex at lower temperatures, except that the second minimum now lies closer to the ground state. The *g*-values estimated for the lowest level of this surface (g_1 = 2.045, g_2 = 2.131, g_3 = 2.433 calculated with k = 0.86) are similar to those at low temperature. The wave functions of the second vibronic energy levels of these surfaces

dx.doi.org/10.1021/ic200554f |*Inorg. Chem.* 2011, 50, 4900–4916

are delocalized, rather than representing the simple interchange of the two longer bond lengths required by the SG model. Such behavior occurs when the barrier height between the wells is low and has been observed for other "dynamic" copper(II) complexes. As discussed for these systems, when the compositions of the upper vibronic levels are considered in conjunction, they do correspond to the expectations of the SG model.[10]

As discussed previously, it is thought that the driving force for the switch of some of the $[Cu(MeOAc)_2(H_2O)_2]$ molecules to a tetragonally compressed form at high temperature is an increase in the magnitude of the axial strain acting on these complexes because of the population of the upper state in the SG equilibrium. The angular form of the potential surface calculated using all parameters as above for the complex at high temperatures (except that S_θ is increased in magnitude to -2000 cm^{-1}), is shown by the blue line in Figure 9. The change in S_θ of -1400 cm^{-1} compared with the tetragonally elongated complex is not much larger than estimates of the axial strain in other complexes where lattice effects induce an axial compression. For instance, S_θ has been estimated as -1000 cm^{-1} in the tetragonally compressed $[CuF_6]^{4-}$ complex present in Cu^{2+}-doped Ba_2ZnF_6.[40] The increase in the magnitude of the axial strain produces a potential surface with a single slightly asymmetric minimum centered close to $\varphi = 180°$, which corresponds to a tetragonally compressed geometry. Unlike the wave functions of the complexes with a tetragonally elongated geometry, these are similar to one another, and show that the unpaired electron resides in an orbital having predominantly d_{z^2} character. The calculated g-values of this form of the complex, $g_1 = 1.993$, $g_2 = 2.259$, $g_3 = 2.364$, are very similar to those estimated using the angular overlap model mentioned previously ($g_1 = 1.990$, $g_2 = 2.261$, $g_3 = 2.366$).

The above calculations are thus consistent with the hypothesis that the basic potential surface of $[Cu(MeOAc)_2(H_2O)_2]$ involves a ground state with long bonds to the methoxy groups and bonds of intermediate length to the water molecules, but with a thermally accessible higher vibronic level where the lengths of these two sets of bonds are interchanged. However, for some complexes, an increase in the magnitude of the axial strain at high temperature produces a surface with just a single, slightly asymmetric minimum corresponding to a tetragonally compressed geometry; a possible reason for this change in strain is discussed below.

Influence of Cooperative Interactions. The behavior of most Cu(II) complexes exhibiting temperature dependent bond lengths and/or EPR spectra can be explained satisfactorily assuming that every complex in a crystal lattice has the same potential surface and that this does not change significantly with temperature. The variation of the spectral and structural properties with temperature is due to the thermal populations of higher vibronic states of the potential surface. An unusual feature of $[Cu(MeOAc)_2(H_2O)_2]$ is that it appears that here at least two types of molecules are present at high temperature with quite distinct potential surfaces. It has been suggested[15] that a similar situation occurs for the $[Cu(D_2O)_6]^{2+}$ ions in $(ND_4)_2[Cu(D_2O)_6](SO_4)_2$. Here the unusual feature is that the higher two g-values and Cu−O bond lengths converge much more rapidly than is expected using the Boltzmann statistics of the simple SG model, and it was proposed that for $(ND_4)_2[Cu(D_2O)_6](SO_4)_2$ the anomalous behavior is due to the development of a population of complexes with a potential surface where the energy difference between the two lower minima is significantly smaller than at low temperature. This implies a lower value of the orthorhombic component of the strain S_ε, and it was proposed that this is caused by the lengthening of the Cu−O(D_2O) bonds in the excited state of the SG-type equilibrium of a neighbor. As this involves a concerted change in structure, the interaction may be designated "cooperative". In $(ND_4)_2[Cu(D_2O)_6](SO_4)_2$, the $[Cu(D_2O)_6]^{2+}$ ions are arranged in the "antiferrodistortive" manner required for this to occur.[15] It was suggested that for a different packing arrangement, such cooperative interactions could affect S_θ rather than S_ε, and we believe that $[Cu(MeOAc)_2(H_2O)_2]$ represents just such an example. It may be noted that the cooperative interactions in the above two complexes are relatively weak as the neighboring complexes are only connected by hydrogen-bonding interactions. Previous studies of cooperative JT interactions have focused on lattices such as $KCuF_3$ and K_2CuF_4 where the metal ion is directly linked to its neighbors by metal−ligand bonds,[41] so the interactions must be considerably stronger. The structural changes that occur upon heating these fluoride lattices are accompanied by crystallographic phases changes,[41] but neither the X-ray nor the EPR data show evidence of a phase change for $[Cu(MeOAc)_2(H_2O)_2]$.

It is relevant to the present discussion that in the EPR study of $[Cu(MeOAc)_2(H_2O)_2]$ at Q-band frequency (~32 GHz), electron exchange between the two molecules in the unit cell was found to be more rapid than the EPR time scale for spectra measured below ~290 K, but above this temperature additional signals due to the individual complexes were resolved.[22] The drop in the rate of electron exchange at high temperature is expected because of the disruption in hydrogen bonding which would accompany the structural changes incumbent in the present model. Moreover, the simultaneous observation of two sets of EPR signals at high temperature implies that the lattice is not homogeneous, and this is consistent with the model developed to interpret the cooperative interactions thought to be present in $(ND_4)_2[Cu(D_2O)_6](SO_4)_2$.[15] This suggests that when a population of complexes having a different potential surface develops, these will tend to form in clusters. It should be noted that the rate of electron exchange between the structural "isomers" in these dynamic equilibria is always faster than the EPR time scale at Q-band frequency, such as the signals due to the compressed and elongated forms of $[Cu(MeOAc)_2(H_2O)_2]$.[22] In an attempt to overcome this limitation, we recorded the EPR spectrum of this compound at various temperatures between 4.2 and 300 K at 406 GHz.[42] However, no further resolution of the spectrum was achieved, though the additional signals due to the individual molecules in the unit cell were observed at temperatures above ~200 K, a somewhat lower threshold than at Q-band frequency.

For $[Cu(MeOAc)_2(H_2O)_2]$, the fact that a population of tetragonally compressed complexes develops at high temperature implies that the magnitude of the axial component of the strain S_θ increases substantially for these complexes. If this is due to a mechanism similar to that proposed for $(ND_4)_2[Cu(D_2O)_6](SO_4)_2$, that is, cooperative interactions involving complexes excited in the SG thermal equilibrium, in order that S_θ rather than S_ε is influenced, the bond lengthening of these excited complexes should occur approximately along the direction of the *short* rather than along the direction of the *long* bonds of neighboring complexes. The crystal packing in $[Cu(MeOAc)_2(H_2O)_2]$ is therefore highly relevant to the present discussion. As discussed previously, the hydrogen atoms of each water molecule are directly hydrogen bonded to the nonbonded oxygen atom of the acetate groups that form the short Cu−O bonds in neighboring complexes. The packing of the complexes is therefore indeed such that excitation in the SG-type equilibrium will tend to increase the magnitude of the axial strain S_θ acting upon neighbors,

as suggested by the above model. Moreover, the relatively small size of the ligands and close packing of the molecules, combined with the fact that no counterions are present, enhances the likelihood that cooperative interactions will be important in $[Cu(MeOAc)_2(H_2O)_2]$.

Each $[Cu(MeOAc)_2(H_2O)_2]$ molecule is hydrogen bonded to six neighbors, the O(4)-H···O(2) contacts being of two kinds; see Figure 4. If the adoption of a compressed geometry is indeed caused by the lengthening of the Cu−O(H_2O) bonds of a tetragonally elongated complex, it might be expected that for each $[Cu(MeOAc)_2(H_2O)_2]$ molecule excited in the SG-type equilibrium, depending on the strength of the cooperative interactions, either two or four neighboring complexes will adopt a compressed tetragonal geometry. It may be seen from Figure 4, that for two neighbors, the hydrogen-bonding interactions are approximately parallel to their C1−O1 bonds, implying strong cooperative interactions, while for the other pair, the hydrogen bonds are nearly perpendicular to the C1−O1 bonds, so that the cooperative interactions are much weaker. In fact, the ratio of the proportion of complexes with a compressed geometry to that with an elongated geometry (with the long bonds to water corresponding to the 240° minimum), is approximately two at low temperature, dropping to ∼1.3 at high temperature (see Figure 6). This suggests that cooperative interactions with just one pair of neighbors dominate in inducing the structural change, and this is consistent with the hydrogen-bonding interactions as mentioned above. The fact that the ratio equals the number predicted by the model at low temperature, but deviates from it at high temperature, is not unreasonable. At low temperature thermal excitation occurs in an essentially uniform lattice consisting of complexes in the low-energy configuration. At high temperature, the lattice comprises a complicated mixture of the three structural forms, so some deviation is not unexpected.

It must be stressed that the model is quite simplistic and can only be expected to give a general picture of what is occurring. As two types of cooperative interactions are to be expected, since two pairs of metal−ligand bonds are involved in the SG-type equilibrium, it could be that two different sets of compressed complexes occur at high temperature. Moreover, only nearest-neighbor interactions have been considered. In practice, the strain interactions on further members of the lattice will also be influenced. Furthermore, the geometries of the upper state of the SG-type equilibrium and the compressed form of $[Cu(MeOAc)_2(H_2O)_2]$ were both estimated assuming a simple picture of the JT distortion, and the true geometries could well deviate somewhat from these idealized forms. Finally, the average metal−ligand bond length increases slightly as the temperature rises, and only the direct effect of this has been taken into account; the possible influence this may have on the forms involved in the thermal equilibria has not been considered. Therefore, while we feel that the above treatment gives an adequate explanation of the behavior of $[Cu(MeOAc)_2(H_2O)_2]$ in general terms, it can only be expected to give an approximate view of the molecular forms present in the compound, and in our view the current data do not warrant a more detailed treatment.

CONCLUSIONS

The drop in axial *g*-shift of $[Cu(MeOAc)_2(H_2O)_2]$ as the temperature rises implies that, on average, the unpaired electron occupies a wave function with ever-increasing d_{z^2} character. This is explained by assuming that while at low temperature the complexes uniformly adopt a tetragonally elongated geometry, at high temperature a thermal equilibrium occurs involving a population of complexes having a tetragonally compressed geometry. This appears to be the first time such behavior has been observed, as other "dynamic" copper(II) complexes involve thermal equilibria between two vibronic states of a set of identical, or near-identical, complexes. Analysis of the *g*-values suggests that the equilibrium involves not only tetragonally compressed complexes but also complexes having a geometry similar to that observed at low temperature, though with the lengths of the bonds to the water and methoxy groups interchanged. The population of each structural type, derived as a function of temperature from the *g*-values predicts Cu−O bond lengths in excellent agreement with the X-ray results if the slight increase in the average Cu−O bond length observed as the temperature rises is included. Calculations using the changes in bond lengths with temperature give broadly similar results. The behavior of the thermal parameters predicted by this model is also in satisfactory agreement with that observed experimentally. The XAFS of the copper(II) and nickel(II) compounds at low temperature yield metal−ligand bond distances similar to those obtained by X-ray diffraction. However, while the XAFS of the nickel(II) compound at high temperature could be interpreted satisfactorily, this was not the case for the copper(II) compound. This is consistent with the proposal that in the latter case two different sets of bond lengths occur, making the structure too complicated for analysis. An infrared combination band observed in the optical spectrum also implies the development of two types of complexes at high temperature.

Potential energy surfaces of the two kinds of molecule thought to be present in $[Cu(MeOAc)_2(H_2O)_2]$ at high temperature have been estimated assuming that these differ in the strain parameters acting on the complexes. At low temperature all the complexes are subjected solely to a strain due predominantly to the inequivalence of the ligand donor atoms. For the complexes that adopt a tetragonally compressed geometry at high temperature, an additional strain "squeezing" the complexes along the direction of the copper(II) carboxylate bonds occurs. It is suggested that this latter strain may be due to cooperative interactions with the complexes excited to the upper vibronic state of the first potential surface, in which the bond lengths to the water and methoxy groups are interchanged. The crystal packing in $[Cu(MeOAc)_2(H_2O)_2]$ is consistent with this hypothesis, and the populations estimated for the different kind of complex at high temperature imply that interactions with one pair of neighboring complexes is dominant. It is pointed out that the model is based upon a number of simplifications, so that it can only be expected to give a broad picture of what is occurring. Hopefully, as experimental methods improve, future measurements of the temperature dependence of the crystal structure and/or XAFS will give more direct and precise information on the molecular structure of the complexes present in $[Cu(MeOAc)_2(H_2O)_2]$ at different temperatures.

ASSOCIATED CONTENT

Supporting Information. X-ray crystallographic data in CIF format for 16 structure determinations of $[Cu(MeOAc)_2(H_2O)_2]$ and 6 of $[Ni(MeOAc)_2(H_2O)_2]$, in addition to XAFS experimental conditions (S-1) and spectra (S-2), and a plot of the average Cu−O bond lengths (S-3). This material is available free of charge via the Internet at http://pubs.acs.org.

dx.doi.org/10.1021/ic200554f |*Inorg. Chem.* 2011, 50, 4900–4916

AUTHOR INFORMATION

Corresponding Author

*E-mail: simmonsc@hawaii.edu (C.J.S.), michael.hitchman@utas.edu.au (M.A.H.), m.riley@uq.edu.au (M.J.R.).

ACKNOWLEDGMENT

Dr. Andrew Ozarowski of the National High Magnetic Field Laboratory, Florida State University, 1800 E. Paul Dirac Drive, Tallahassee, Florida 32310 is thanked for undertaking the high-frequency EPR measurements reported here.

REFERENCES

(1) (a) Bersuker, I. B. *The Jahn-Teller Effect and Vibronic Interactions in Modern Chemistry*; Plenum: New York, 1984. (b) Bersuker, I. B. *The Jahn-Teller Effect*; Cambridge University Press: Cambridge, 2006. (c) Reinen, D.; Atanasov, M. *Chem. Phys.* **2009**, *97*, 451.

(2) Hitchman, M. A. *Comments Inorg. Chem.* **1994**, *15*, 197–254.

(3) (a) Keller, H.; Bussmann-Holder, A.; Müller, K. A. *Mater. Today* **2009**, *11*, 38–46. (b) Phillips, J. C. *Proc. Natl. Acad. Sci. U.S.A.* **2009**, *106*, 15534–37.

(4) (a) Bacci, M. *New J. Chem.* **1993**, *17*, 67–70. (b) Gray, H. B.; Molstroem, B. G.; Williams, R. J. *J. Biol. Inorg. Chem.* **2000**, *5*, 551–559.

(5) Riley, M. J.; Hitchman, M. A.; Reinen, D. *Chem. Phys.* **1986**, *102*, 11–28.

(6) Falvello, L. R. *J. Chem. Soc., Dalton Trans.* **1997**, 4463–4475.

(7) Silver, B.; Getz, D. *J. Chem. Phys.* **1974**, *61*, 638–650.

(8) Riley, M. J.; Hitchman, M. A.; wan Mohammed, A. *J. Chem. Phys.* **1987**, *87*, 3766–3778.

(9) Riley, M. J.; Hitchman, M. A.; Reinen, D.; Steffen, G. *Inorg. Chem.* **1988**, *27*, 1924–1934.

(10) Bebendorf, J.; Bürgi, H.-B.; Gamp, E.; Hitchman, M. A.; Murphy, A.; Reinen, D.; Riley, M. J.; Stratemeier, H. *Inorg. Chem.* **1996**, *359*, 7419–7429.

(11) Dobe, C.; Noble, C.; Carver, G.; Treggenna-Piggott, P. L. W.; McIntyre, G. J.; Barra, A.-L.; Neels, A.; Janssen, S.; Juranyi, F. *J. Am. Chem. Soc.* **2004**, *126*, 16639–16652.

(12) (a) Tucker, D.; White, P. S.; Trojan, K. L.; Kirk, M. L.; Hatfield, W. E. *Inorg. Chem.* **1991**, *30*, 823–826.13. (b) Ellis, P. J.; Freeman, H. C.; Hitchman, M. A.; Reinen, D.; Wagner, B. *Inorg. Chem.* **1994**, *33*, 1249–1250.

(13) Riley, M. J. *Top. Current Chem.* **2001**, *214*, 57–80.

(14) (a) Masters, V. M.; Riley, M. J.; Hitchman, M. A. *Inorg. Chem.* **2001**, *40*, 843–849. (b) Figgis, B. N.; Iverson, B. B.; Larsen, F. K.; Reynolds, P. *Acta Crystallogr.* **1993**, *B49*, 794–806.

(15) Hitchman, M. A.; Maaskant, W.; van der Plas, J.; Simmons, C. J.; Stratemeier, H. *J. Am. Chem. Soc.* **1999**, *121*, 1488–1501.

(16) Alimohammadi, Z.; Rahemi, H.; Golzan, M.; Tayyari, S. F.; Riley, M. J. *J. Mol. Model.* **2009**, *15*, 391–395.

(17) (a) Forrest, J. G.; Prout, C. K.; Rossotti, F. J. C. *Chem. Commun.* **1966**, 658–660. (b) Prout, C. K.; Armstrong, R. A.; Carruthers, J. R.; Forrest, J. G.; Murray-Rust, P.; Rossotti, F. J. C. *J. Chem. Soc. A* **1968**, 2791–2813.

(18) Hathaway, B. J. *Struct. Bonding (Berlin)* **1984**, *57*, 54–118.

(19) Prout, C. K.; Edwards, A.; Mtetwa, V.; Murray, J.; Saunders, J. F.; Rossotti, F. J. C. *Inorg. Chem.* **1997**, *36*, 2820–2825.

(20) Bew, M. J.; Billing, D. E.; Dudley, R. J.; Hathaway, B. J. *J. Chem. Soc. A* **1970**, 2640–2644.

(21) Dawson, K.; Hitchman, M. A.; Prout, K. C.; Rossotti, F. J. C. *J. Chem. Soc., Dalton Trans.* **1972**, 1509–1519.

(22) Jakob, B.; Reinen, D. *Z. Naturforsch.* **1987**, *42b*, 1500–1506.

(23) Pilbrow, J. R. *Transition Ion Electron Paramagnetic Resonance*; Clarendon Press: Oxford, 1990.

(24) The structure of this compound has already been reported at room temperature; see ref 19 and references therein.

(25) (a) Otwinowski, Z.; Minor, W. *Methods in Enzymology*; Carter, C. W. Jr.; Sweet, R. M., Eds.; Academic Press: New York, 1997; Vol. 276, pp 307−326. (b) *teXsan, Crystal Structure Analysis Package*; Molecular Structure Corp.: The Woodlands, TX, 1992; v. 1.06. (c) *PLATON for Windows*; Farrugia, L. J., University of Glasgow and Spek, A. L., Utrecht University.

(26) Hitchman, M. A.; Riley, M. J. *Inorganic Electronic Structure and Spectroscopy*; Solomon, E. I., Lever, A. J. P., Eds.; J. Wiley and Sons: New York, 1999; Vol. 1, Chapter 4, p 227.

(27) Hitchman, M. A.; Waite, T. D. *Inorg. Chem.* **1976**, *15*, 2150–2154.

(28) Nakamoto, K. *Infrared and Raman Spectra of Inorganic and Coordination Compounds*, 3rd ed.; Wiley & Sons: New York; p 227.

(29) Gerloch, M. *CAMMAG, a FORTRAN program for AOM calculations*; University of Cambridge: Cambridge, U.K.

(30) McDonald, R. G.; Hitchman, M. A. *Inorg. Chem.* **1990**, *29*, 3081–3088.

(31) Figgis, B. N.; Hitchman, M. A. *Ligand Field Theory and its Applications*; Wiley-VCH: New York, 2000; p 69.

(32) (a) Ref 26, p.70. (b) Hitchman, M. A.; Kwan, L.; Engelhardt, L. M.; White, A. H. *J. Chem. Soc., Dalton Trans.* **1987**, 457–465.

(33) Ref 26, p. 64.

(34) Bürgi, H. B. *Acta Crystallogr.* **1989**, *B45*, 383–390.

(35) Stebler, M.; Bürgi, H. B. *J. Am. Chem. Soc.* **1987**, *109*, 1395–1401.

(36) Masters, V. M., Ph.D. Thesis, University of Queensland, Queensland, Australia, 2001.

(37) Ravel, B.; Newville, M. *J. Synchrotron Radiat.* **2005**, *12*, 537–541.

(38) Hitchman, M. A.; Yablokov, Y. V.; Petrashen, V. E.; Augustyniak-Jablokov, M. A.; Stratemeier, H.; Riley, M. J.; Lukaszewicz, K.; Tomaszewski, P. E.; Pietraszko, A. *Inorg. Chem.* **2002**, *41*, 229–238.

(39) Hitchman, M. A.; Hockless, D. C. R.; Skelton, B. W.; Stratemeier, H.; White, A. H. *Z. Anorg. Allg. Chem.* **2007**, *633*, 2004–2008.

(40) Steffen, G.; Reinen, D.; Stratemeier, H.; Riley, M. J.; Hitchman, M. A.; Mathies, H. E.; Recker, K.; Wallrafen, F.; Niklas, J. R. *Inorg. Chem.* **1990**, *29*, 2123–2131.

(41) Reinen, D.; Atanasov, M. *Magn. Reson. Rev.* **1991**, *15*, 167, and references therein.

(42) The measurements of the high-frequency EPR spectra were made by Dr. Andrew Ozarowski of the National High Magnetic Field Laboratory, Florida State University, 1800 E. Paul Dirac Drive, Tallahassee, Florida 32310.